RESEARCH ARTICLES

TRANSLATION

Real-time quantification of single RNA translation dynamics in living cells

Tatsuya Morisaki,[1] Kenneth Lyon,[1] Keith F. DeLuca,[1] Jennifer G. DeLuca,[1] Brian P. English,[2] Zhengjian Zhang,[2] Luke D. Lavis,[2] Jonathan B. Grimm,[2] Sarada Viswanathan,[2] Loren L. Looger,[2] Timothee Lionnet,[2] Timothy J. Stasevich[1]*

Although messenger RNA (mRNA) translation is a fundamental biological process, it has never been imaged in real time in vivo with single-molecule precision. To achieve this, we developed nascent chain tracking (NCT), a technique that uses multi-epitope tags and antibody-based fluorescent probes to quantify protein synthesis dynamics at the single-mRNA level. NCT reveals an elongation rate of ~10 amino acids per second, with initiation occurring stochastically every ~30 seconds. Polysomes contain ~1 ribosome every 200 to 900 nucleotides and are globular rather than elongated in shape. By developing multicolor probes, we showed that most polysomes act independently; however, a small fraction (~5%) form complexes in which two distinct mRNAs can be translated simultaneously. The sensitivity and versatility of NCT make it a powerful new tool for quantifying mRNA translation kinetics.

At the core of all gene regulatory networks are the processes of DNA transcription and RNA translation. Although transcription is now regularly quantified in real time in vivo with single-gene resolution (*1*, *2*), the same cannot be said for translation. In principle, fluorescent tags such as green fluorescent protein (GFP) could be used to do this, but in practice, these tags take too long to fluoresce or their signals are too weak to visualize translation of a single RNA in real time (*3*). Recently, some of these problems were overcome by using a RNA biosensor that is dislodged by translating ribosomes (*4*). However, fluorescence is lost on the first round of translation with this assay, so ongoing translation dynamics cannot be visualized.

Developing a method to visualize the translation of single mRNAs in living cells

To visualize translation of a single RNA in real time, we developed a system based on bright photostable small-molecule dyes, antibody enhancement, and multi-epitope protein tags. We constructed a plasmid encoding the large nuclear protein KDM5B, N-terminally tagged with a 10× FLAG tag (which we refer to as the spaghetti monster, SM) (*5*) and containing a 24× MS2 tag (*6*) in the 3′ untranslated region (UTR) (Fig. 1A). The FLAG SM tag created a highly avid site for binding of fluorescently labeled fragments of antibody to FLAG (anti-FLAG Fab), whereas the MS2 stem-loop repeat allowed visualization with labeled MS2 coat protein (MCP) (*2*, *6*) (Fig. 1B). We transiently transfected this plasmid into U2OS cells that were subsequently bead-loaded with Cy3-labeled anti-FLAG Fab and Halo-tagged MCP [labeled with the far-red JF646 fluorophore (*7*)]. Twenty-four hours after transfection, MCP marked mRNA in the cytoplasm and Fab marked KDM5B in the nucleus, suggesting that neither the FLAG SM tag nor the presence of Fab interfered with mRNA and KDM5B production and localization (Fig. 1C). To see how soon Fab could mark protein, we imaged ~6 hours after transfection. At this early time, Fab only lightly marked the nucleus, suggesting that very little KDM5B had been synthesized (Fig. 1D). Fab also colocalized and co-moved with many MCP-labeled mRNAs in the cytoplasm (Fig. 1, D and E, and movie S1). These bright co-moving spots displayed RNA-like diffusivity, were very stable—lasting for 2 hours or more (movie S2)—and could only be seen in the cytoplasm of cells that were both transfected with FLAG SM–tagged KDM5B and bead-loaded with Fab.

We wondered whether the co-moving protein-mRNA spots were bona fide translation sites. To test this, we treated cells with 50 μg/ml of puromycin, an inhibitor of translation that releases nascent chains from ribosomes (*8*). Within minutes of drug addition, the number of co-moving spots dropped exponentially (Fig. 1, F and G, and movie S3). By tracking co-moving spots, we could see the disappearance of Fab-labeled protein, despite the persistence of the mRNA (Fig. 1F). The time of complete protein disappearance varied among different mRNAs, but there was a well-defined exponential decay in the number of protein spots (Fig. 1G). To further confirm that protein-mRNA spots were translation sites, we treated cells with 4 μg/ml cycloheximide to slow elongation and load more ribosomes per transcript, and the spots became brighter (fig. S1). Together, these data suggest that the co-moving spots were indeed translation sites.

KDM5B is a large protein (1544 amino acids), so its translation should be relatively easy to detect. To see whether we could also detect translation of smaller proteins, we constructed two plasmids (Fig. 2A) encoding either β-actin (374 amino acids) or the core histone H2B (125 amino acids). As with KDM5B, neither the FLAG SM tag nor Fab disturbed the localization of these proteins (Fig. 2, B and C), and Western blots confirmed that tagged proteins were of the expected length (fig. S2). Furthermore, we could again observe translation sites ~6 hours after transient transfection (Fig. 2D and movies S4 and S5), indicating that our system is useful for imaging the translation of protein-coding genes of varying sizes.

Nascent chain tracking to quantify polysome mobility and size

We tracked translation of single molecules by using a technique that we call nascent chain tracking (NCT). With NCT, we followed individual H2B, β-actin, and KDM5B translation sites for hundreds to thousands of seconds in full cell volumes (300 time points × 2 colors × 13 *z* planes = 7800 images per movie). We adjusted laser powers to focus exclusively on translation sites rather than on fully translated single protein products (which could interfere with tracking). As shown in the inset of Fig. 2D, this allowed us to accurately compare (i) the appearance frequency and brightness, (ii) the mobility, and (iii) the size of translation sites. Of these parameters, frequency and brightness varied the most, tending to increase with construct length. We detected the translation of 86 ± 2% of KDM5B mRNA but just 19 ± 4% of β-actin mRNA and 4 ± 1% of H2B mRNA (error, SEM) (Fig. 2E). Furthermore, KDM5B translation sites, as marked by Fab, were over 1.5 times as bright as β-actin sites, which themselves were nearly 1.5 times as bright as H2B sites (Fig. 2F).

One explanation for the difference in brightness in translation sites could be a difference in the number of nascent peptide chains per mRNA, as would be the case in polysomes (*9*). To determine precisely how many nascent chains exist per site, we calibrated fluorescence by imaging a new β-actin plasmid containing a single 1× FLAG tag rather than the 10× FLAG SM tag (fig. S3A). With this plasmid, only one Fab can be bound per peptide chain, allowing a direct comparison between translation site fluorescence and single Fab fluorescence. By imaging cells transfected with this plasmid at high laser powers, both single Fabs and translation sites could be detected and tracked (fig. S3, B and C), revealing translation sites to be on average 3.1 ± 0.5 times as bright as single Fabs (fig. S3D). We therefore estimate that there are 3.1 ± 0.5 nascent peptide chains per β-actin translation site, 2.1 ± 0.4 per H2B site, and 5.1 ± 0.9 per KDM5B site (Fig. 2F, right axis). Combining these data and assuming one ribosome per

[1]Department of Biochemistry and Molecular Biology and Institute for Genome Architecture and Function, Colorado State University, Fort Collins, CO, USA. [2]Janelia Research Campus, Howard Hughes Medical Institute, Ashburn, VA, USA.
*Corresponding author. Email: tim.stasevich@colostate.edu

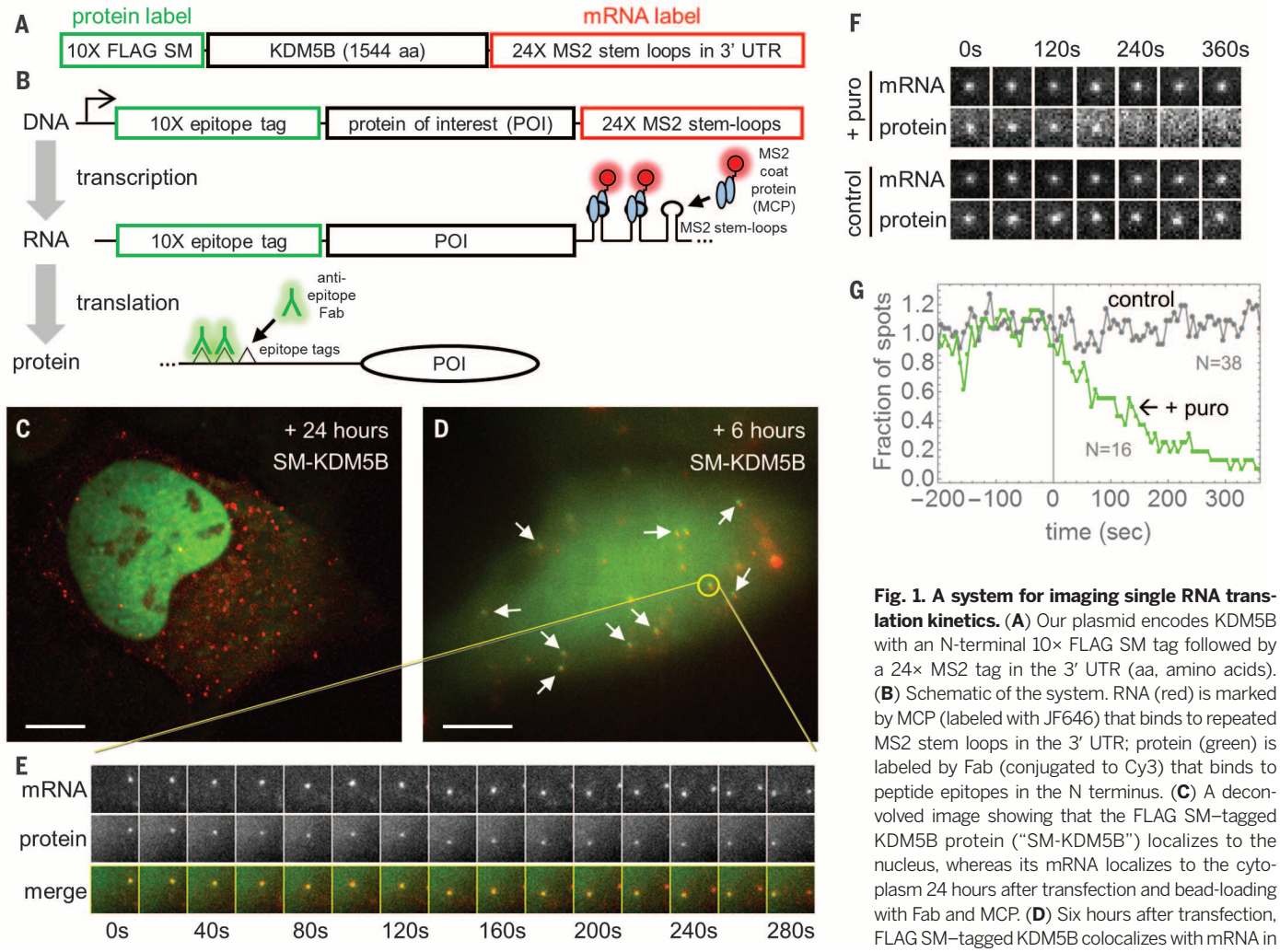

Fig. 1. A system for imaging single RNA translation kinetics. (**A**) Our plasmid encodes KDM5B with an N-terminal 10× FLAG SM tag followed by a 24× MS2 tag in the 3′ UTR (aa, amino acids). (**B**) Schematic of the system. RNA (red) is marked by MCP (labeled with JF646) that binds to repeated MS2 stem loops in the 3′ UTR; protein (green) is labeled by Fab (conjugated to Cy3) that binds to peptide epitopes in the N terminus. (**C**) A deconvolved image showing that the FLAG SM–tagged KDM5B protein ("SM-KDM5B") localizes to the nucleus, whereas its mRNA localizes to the cytoplasm 24 hours after transfection and bead-loading with Fab and MCP. (**D**) Six hours after transfection, FLAG SM–tagged KDM5B colocalizes with mRNA in punctae (arrows). (**E**) Example co-movement of FLAG SM–tagged KDM5B and mRNA punctae circled in yellow in (D). (**F**) Addition of puromycin (50 μg/ml) leads to a loss of the FLAG SM–tagged KDM5B signal in punctae; this does not occur in control cells loaded with vehicle. (**G**) Quantification of the loss of the FLAG SM–tagged KDM5B signal from punctae (lower green curve) in a single cell as a function of time after addition of puromycin (which takes effect at 0 s), compared with the signal from a control cell (upper gray curve). Curves are normalized to pre-puromycin levels. Scale bars, 10 μm.

nascent chain, we conclude that detected translation sites are polysomes that can contain as few as one ribosome every 900 mRNA bases or as many as one ribosome every 200 mRNA bases.

In addition to differences in their brightness, NCT also exposed differences in the mobility of polysomes. We quantified this by measuring the mean squared displacement of tracked polysomes as a function of time. For the nuclear proteins H2B and KDM5B, mobility was modeled well by diffusion. Not only did displacement increase linearly with time for at least 20 s, the less massive H2B polysomes also moved significantly faster than KDM5B polysomes (Fig. 2G). In contrast, β-actin polysomes displayed constrained diffusion, with jump sizes that were initially between those of KDM5B and H2B (consistent with diffusion) but that ultimately lagged behind both at longer times. This constrained movement of β-actin could be due to interactions with cytoplasmic binding partners. Despite these trends, there was substantial variability in mobility between mRNA, so that we sometimes saw rapidly moving KDM5B polysomes (up to 6 $\mu m^2/s$) and nearly immobile H2B polysomes (~0.01 $\mu m^2/s$; fig. S4). This made it nearly impossible to identify a translated mRNA based on mobility alone, implying that the translation machinery only weakly alters mRNA movement in our system.

Unlike their brightness and mobility, the size of polysomes was less variable between constructs. To quantify sizes, we measured the distance between the 3′ UTR of polysomal mRNA (labeled with MCP) and the nascent peptide chains (labeled with Fab). The fluorescence from polysomes was within diffraction-limited spots, so we determined their mean positions with superresolution by using Gaussian fitting (fig. S5). According to hairpin models of polysome organization (*10*), this distance should grow as the length of the mRNA grows. Instead, we found that the distance was shortest in KDM5B polysomes, typically around 65 nm, compared with 85 nm for H2B and 105 nm for β-actin (Fig. 2H). This suggests that the polysomes that we imaged are organized in a globular shape rather than an elongated shape, consistent with recent atomic force microscopy images (*11*).

Extracting translation kinetics from NCT data

Having measured the basic physical properties of polysomes, we next focused on translation kinetics. In particular, we wondered how the number of ribosomes in polysomes is controlled. This number reflects a balance between incoming and outgoing ribosomes and therefore depends on the ribosome elongation rate. One way to noninvasively estimate this rate is to examine the correlation of fluctuations in NCT data by means of fluorescence correlation spectroscopy (FCS), similar to how transcription elongation rates have been measured by using MS2 fluorescence fluctuations (*12*). Before doing so, however, we needed to ensure that Fabs would bind polysomes quickly and irreversibly on the time scale of translation. If not, their dynamics would contribute to the

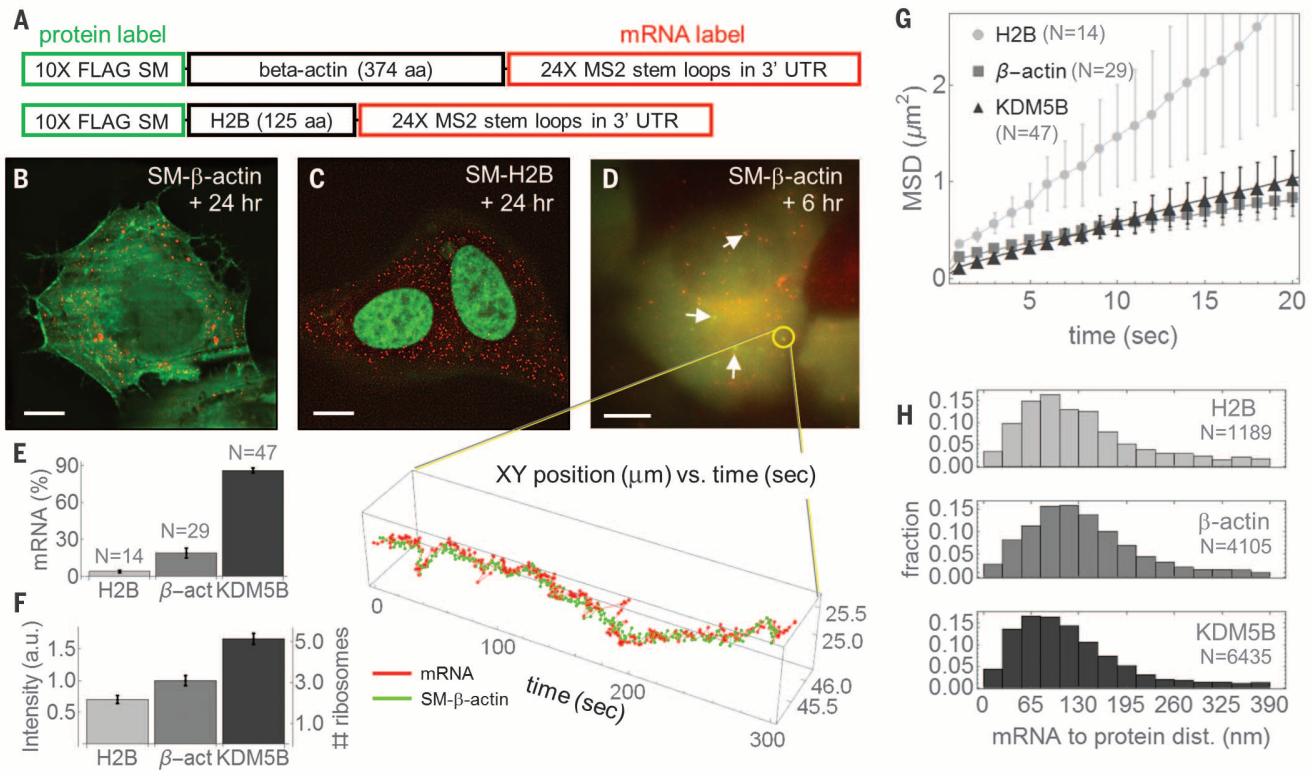

Fig. 2. Quantifying the mobility, ribosomal content, and structure of translation sites. (**A**) Plasmids encoding β-actin (SM-β-actin) and H2B (SM-H2B), analogous to the FLAG SM–tagged KDM5B construct in Fig. 1A. (**B** and **C**) Deconvolved images showing that SM-β-actin [(B), green] and SM-H2B [(C), green] localize to the cytoplasm and nucleus, respectively, whereas their mRNAs (red) both localize to the cytoplasm 24 hours after transfection and bead-loading with Fab and MCP. (**D**) Six hours after transfection, SM-β-actin translation sites can be seen (arrows) and tracked (yellow circle and inset). (**E** and **F**) Quantification of the frequency (E) and intensity (F) of translation sites. Normalization to the number of ribosomes is shown on the right axis in (F) (a.u., arbitrary units). (**G**) Measured mean squared displacements (MSD) of tracked polysomes as a function of time. (**H**) Histograms of the Gaussian fit distances between mRNA and protein in tracked polysomes. Error bars show SEM. Scale bars, 10 μm.

fluctuations, and this would distort our FCS measurements of elongation times.

To measure how quickly Fabs bind polysomes, we microinjected them into cells transfected 6 hours earlier with our KDM5B construct and preloaded with MCP. Just 3 s after microinjection (as soon as we could image), many polysomes were labeled by Fab, implying that the binding time is less than 3 s (Fig. 3, A and B). To measure the lifetime of Fab binding, we performed fluorescence recovery after photobleaching (FRAP) experiments in cells transfected with the H2B construct and bead-loaded with Fab and MCP 24 hours earlier. We chose H2B because it is known to remain bound for hours (*13*, *14*), so any fluorescence recovery on the time scale of minutes would be exclusively due to Fab turnover. As Fig. 3C shows, there was little FRAP recovery in 4 min, implying that most Fabs are bound much longer. These binding kinetics (Fig. 3D) make Fabs ideal tools for measuring translation elongation times on time scales ranging from ~10 s to ~5 min.

Knowing the limits of Fab, we analyzed the fluorescence fluctuations of polysomes by extracting their intensity time series from our tracking data. We began with KDM5B polysomes because these were the brightest and most numerous. The intensity of polysomes fluctuated with time (Fig. 3E), reflecting changes in the number of elongating ribosomes. From each intensity time series, we computed the correlation curve, and we averaged these together. There was high variability among mRNAs (fig. S6), but the average correlation curve revealed a clear linear drop in correlation that went to zero at 149 ± 20 s (Fig. 3F, upper panel). In direct analogy to transcription correlation analyses (*12*), the time at which the correlation drops to zero marks the total elongation dwell time. To confirm this, we treated cells with 100 μg/ml of cycloheximide to stall translation. As expected, the correlation disappeared (fig. S7 and movies S6 and S7).

To corroborate these measurements, we performed FRAP on KDM5B polysomes. We photobleached a large section of the cytoplasm where many polysomes were present (fig. S8). By tuning the powers of the photobleaching laser, we could selectively photobleach just the Fab, leaving the mRNA bright. This allowed us to monitor the fluorescence recovery of the relatively slower-moving polysomes. On average, polysomes recovered 80 to 90% of their fluorescence in 125 to 180 s, although there was again high variability among mRNAs, just as with FCS. Nevertheless, the average recovery time was on the same time scale as our FCS measurements.

Given this consistency, we next performed FCS on the shorter β-actin and H2B constructs. Again, the correlation curves were linear and went to zero at distinct elongation dwell times, whereas random background spots showed no correlations from frame to frame (fig. S9). As expected, the dwell times decreased with mRNA length, being 32 ± 9 s for β-actin and just 16 ± 7 s for H2B (Fig. 3F, lower panels). Importantly, for all constructs, the correlation vanished at times greater than the dwell time. This implies that initiation is random, so there is no memory between initiation events, similar to transcriptional initiation (*12*) and in contrast to bursting (*15*, *16*).

To calculate the elongation rate, we divided the length of the encoded protein by the elongation dwell time of each construct. The calculated rates were all within error (Fig. 3G), yielding a single consistent elongation rate of 10 ± 2.3 amino acids/s, which is fairly close to what has been measured using genome-wide ribosomal profiling (5.6 amino acids/s) (*17*, *18*). The difference is probably due to single-molecule variability (as shown in figs. S4 and S6) or differences in mRNA sequence and codon usage (*19*).

With a consistent elongation rate, we can unify our observations. First, assuming KDM5B elongation occurs at 10 ± 2.3 amino acids/s, a new

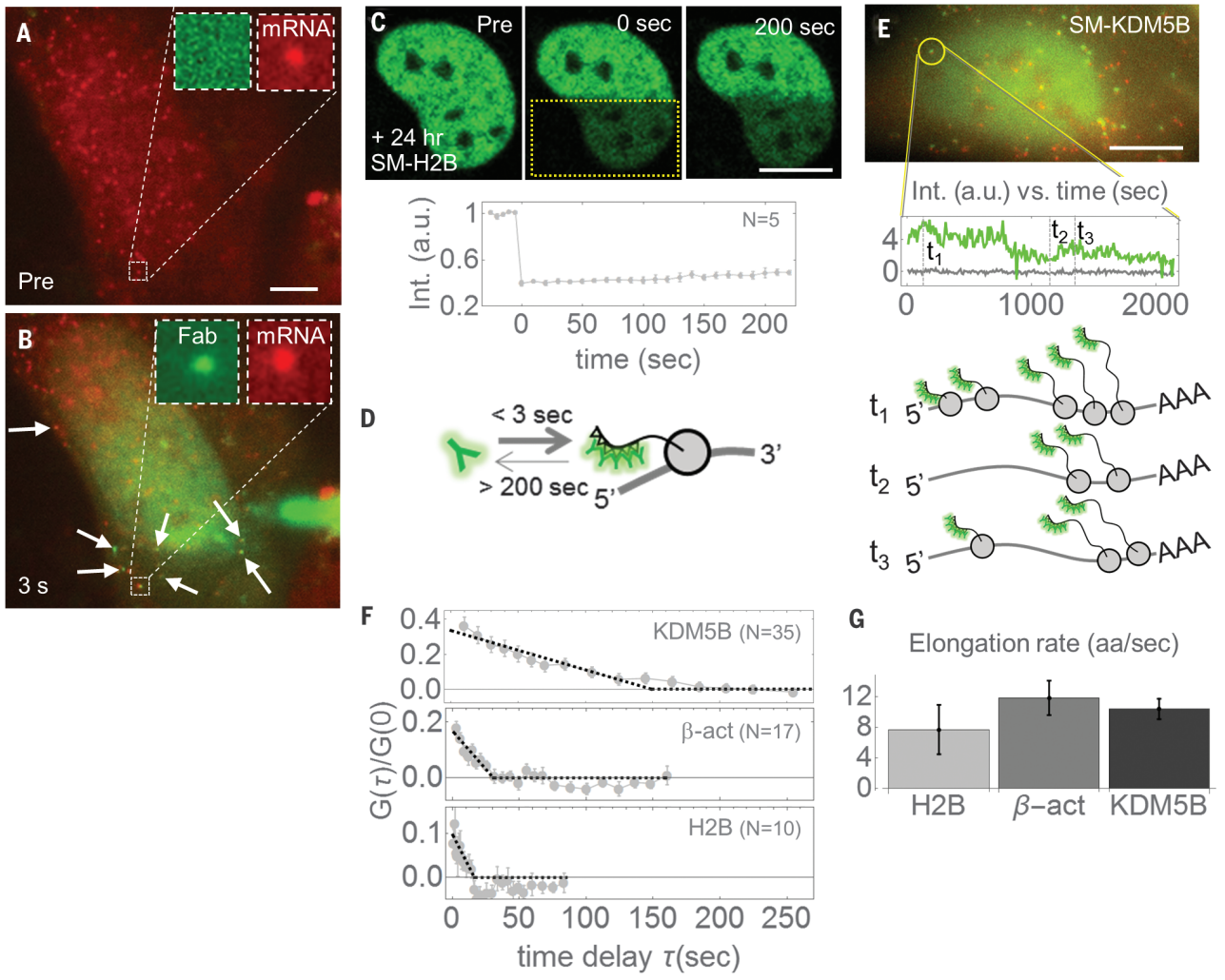

Fig. 3. Quantifying the translational kinetics of tracked polysomes. (**A**) Sample cell transfected with FLAG SM–tagged KDM5B and loaded with MCP before Fab microinjection. Many mRNAs (red) can be seen. Their fluorescence does not bleed into the green channel (inset). (**B**) Three seconds after microinjection, Fabs (green) co-localize with mRNAs (arrows and inset). The site of microinjection can be seen on the right (bright green smear). (**C**) Sample FRAP experiment on a cell transfected with SM-H2B and bead-loaded with MCP and Fab 24 hours earlier. There is little recovery in 200 s (lower curve; int., intensity). Error bars show SEM. (**D**) A cartoon of results from (A) to (C) showing fast on rates and slow off rates for Fab (green Y shapes) binding to SM epitopes (triangles) as they emerge from a ribosome (circle) translating mRNA (thick line). (**E**) The intensity of a tracked FLAG SM–tagged KDM5B polysome (yellow circle and inset) can be measured as a function of time. The cartoon below shows how movement of ribosomes along mRNA and the emergence of elongating peptide chains can produce intensity fluctuations at the indicated times t_1, t_2, and t_3 (AAA, poly-A tail). (**F**) The average correlation curves calculated from intensity fluctuation data for each construct (error bars show SEM; *G*, autocorrelation function). The time at which the correlation hits zero can be obtained from fits (dashed lines) to estimate the elongation dwell time. (**G**) Calculated elongation rates (amino acids per second) from fits in (F) (error bars show 95% confidence intervals). Scale bars, 10 μm.

ribosome would have to initiate on average every 30 ± 9 s to maintain the measured 5.1 ± 0.9 ribosomes per polysome. From this we can predict that 96 ± 3% of KDM5B mRNA will be translated by polysomes, 3.1 ± 2.5% of KDM5B mRNA will be translated by a single ribosome, and 0.6 ± 0.6% will be untranslated. Moreover, using the same initiation and elongation rates for the other constructs (because they have the same 5′ and 3′ UTRs), we can predict that 35 ± 9% of β-actin mRNA will be translated by polysomes containing 2.5 ± 0.1 ribosomes on average (36 ± 2% translated by single ribosomes and 29 ± 7% untranslated), whereas just 6.5 ± 2.5% of H2B mRNA will be translated by polysomes containing 2.2 ± 0.1 ribosomes on average (27 ± 3% translated by single ribosomes and 66 ± 5% untranslated).

These predictions (detailed in the supplementary materials and summarized in figs. S10 and S11) are consistent with our earlier measurements of polysomes (19 ± 4% of β-actin mRNA containing 3.1 ± 0.5 ribosomes and 4 ± 1% of H2B mRNA containing 2.1 ± 0.4 ribosomes). They are also in agreement with independent measurements of the number of ribosomes per polysome obtained by polysome profiling (figs. S10 and S11). Although we found a lower density of ribosomes within polysomes than others have (*20*, *21*), the consistency of our live-cell and biochemical data suggests that the difference is due to mRNA variability rather than to experimental stress that might artificially lower the density. In particular, other mRNAs with different 5′ and 3′ architectures (*22*, *23*) will probably have different polysome occupancies and dynamics, depending not only on the balance of elongation and initiation but also on the metabolic status of the cell and the local environment.

Simultaneous multicolor imaging of distinct mRNAs being translated in a single cell

One advantage of using Fab to mark translation sites is the large number of high-affinity antibodies for multicolor applications. To demonstrate this,

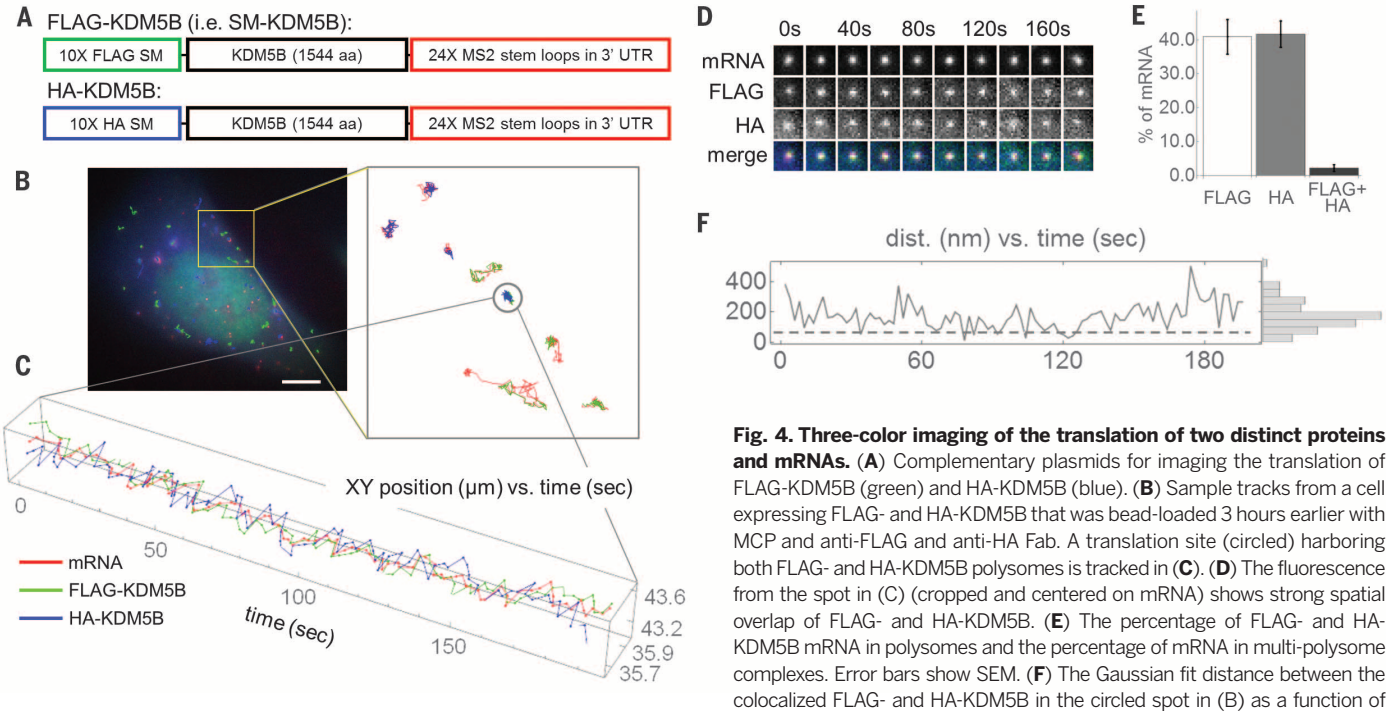

Fig. 4. Three-color imaging of the translation of two distinct proteins and mRNAs. (**A**) Complementary plasmids for imaging the translation of FLAG-KDM5B (green) and HA-KDM5B (blue). (**B**) Sample tracks from a cell expressing FLAG- and HA-KDM5B that was bead-loaded 3 hours earlier with MCP and anti-FLAG and anti-HA Fab. A translation site (circled) harboring both FLAG- and HA-KDM5B polysomes is tracked in (**C**). (**D**) The fluorescence from the spot in (C) (cropped and centered on mRNA) shows strong spatial overlap of FLAG- and HA-KDM5B. (**E**) The percentage of FLAG- and HA-KDM5B mRNA in polysomes and the percentage of mRNA in multi-polysome complexes. Error bars show SEM. (**F**) The Gaussian fit distance between the colocalized FLAG- and HA-KDM5B in the circled spot in (B) as a function of time. The distribution of these distances is shown on the right. It peaks at ~130 nm, twice the distance reported in Fig. 2H between KDM5B nascent chains and mRNA in a single polysome (~65 nm, dashed line).

we generated new Fabs from hemagglutinin (HA) antibodies and labeled these with Alexa488 dye. In parallel, we engineered a new KDM5B construct with a 10× HA SM tag (HA-KDM5B) (*5*) to complement FLAG SM–tagged KDM5B (hereafter, FLAG-KDM5B), as shown in Fig. 4A. As a first application of this technology, we wanted to test whether polysomes interact with each other to form higher-order structures that can translate two distinct mRNAs at the same time. For this, we cotransfected cells with HA- and FLAG-KDM5B and bead-loaded them with MCP and anti-HA and anti-FLAG Fab. As anticipated, cotransfected cells contained two types of polysomes in equal fractions (Fig. 4, B to E), one type labeled by anti-HA Fab (HA-KDM5B) and the other labeled by anti-FLAG Fab (FLAG-KDM5B) (Fig. 4B and movie S8). For the most part, there was little interaction between the two, providing direct evidence that the vast majority of KDM5B polysomes act independently of one another. However, a small fraction (~5%) of KDM5B polysomes formed complexes that co-moved for hundreds of seconds (Fig. 4, C and D, and fig. S12) and that produced both HA- and FLAG-tagged nascent peptide chains. By measuring the distance between the nascent HA and FLAG chains, we found the complexes to be roughly twice the size of a single polysome (Fig. 4F), suggesting that the component polysomes remain compartmentalized. These complexes could reflect a more general strategy to either assemble higher-order complexes cotranslationally (*24*) or co-regulate the expression of two genes.

This work is similar to a companion study by Wu *et al.* (*25*) that combined the SunTag (*26*) with MS2 to image single mRNA translation kinetics in live cells. Their measurements and our measurements of translation elongation and initiation rates are within a factor of 2, indicating that the general approach is reproducible between laboratories. Although the techniques are similar, the combination of anti-FLAG Fab and anti-HA Fab enables multicolor experiments that are not possible with the SunTag system. Also, the FLAG and HA epitopes (8 and 9 amino acids, respectively) are just over one-third the size of the SunTag epitope (22 amino acids), so spatio-temporal resolution can be up to three times as good and imaging is potentially less invasive. These advantages will make NCT a powerful new tool for detecting, tracking, and quantifying translation dynamics and for dissecting gene regulatory networks in vivo.

REFERENCES AND NOTES

1. G. L. Hager, J. G. McNally, T. Misteli, *Mol. Cell* **35**, 741–753 (2009).
2. X. Darzacq *et al.*, *Annu. Rev. Biophys.* **38**, 173–196 (2009).
3. J. A. Chao, Y. J. Yoon, R. H. Singer, *Cold Spring Harb. Perspect. Biol.* **4**, a012310–a012310 (2012).
4. J. M. Halstead *et al.*, *Science* **347**, 1367–1671 (2015).
5. S. Viswanathan *et al.*, *Nat. Methods* **12**, 568–576 (2015).
6. E. Bertrand *et al.*, *Mol. Cell* **2**, 437–445 (1998).
7. J. B. Grimm *et al.*, *Nat. Methods* **12**, 244–250 (2015).
8. G. Blobel, D. Sabatini, *Proc. Natl. Acad. Sci. U.S.A.* **68**, 390–394 (1971).
9. J. R. Warner, A. Rich, C. E. Hall, *Science* **138**, 1399–1403 (1962).
10. A. K. Christensen, C. M. Bourne, *Anat. Rec.* **255**, 116–129 (1999).
11. G. Viero *et al.*, *J. Cell Biol.* **208**, 581–596 (2015).
12. D. R. Larson, D. Zenklusen, B. Wu, J. A. Chao, R. H. Singer, *Science* **332**, 475–478 (2011).
13. H. Kimura, P. R. Cook, *J. Cell Biol.* **153**, 1341–1354 (2001).
14. F. Mueller, T. Morisaki, D. Mazza, J. G. McNally, *Biophys. J.* **102**, 1656–1665 (2012).
15. D. R. Larson, R. H. Singer, D. Zenklusen, *Trends Cell Biol.* **19**, 630–637 (2009).
16. J. Yu, J. Xiao, X. Ren, K. Lao, X. S. Xie, *Science* **311**, 1600–1603 (2006).
17. N. T. Ingolia, S. Ghaemmaghami, J. R. S. Newman, J. S. Weissman, *Science* **324**, 218–223 (2009).
18. N. T. Ingolia, L. F. Lareau, J. S. Weissman, *Cell* **147**, 789–802 (2011).
19. J.-R. Yang, X. Chen, J. Zhang, *PLOS Biol.* **12**, e1001910 (2014).
20. R. D. Palmiter, *Cell* **4**, 189–197 (1975).
21. R. Jackson, N. Standart, *RNA* **21**, 652–654 (2015).
22. G. S. Wilkie, K. S. Dickson, N. K. Gray, *Trends Biochem. Sci.* **28**, 182–188 (2003).
23. N. Sonenberg, A. G. Hinnebusch, *Cell* **136**, 731–745 (2009).
24. Y.-W. Shieh *et al.*, *Science* **350**, 678–680 (2015).
25. B. Wu, C. Eliscovich, Y. J. Yoon, R. H. Singer, *Science* **352**, 1430–1435 (2016).
26. M. E. Tanenbaum, L. A. Gilbert, L. S. Qi, J. S. Weissman, R. D. Vale, *Cell* **159**, 635–646 (2014).

ACKNOWLEDGMENTS

This work was supported by start-up funds from Colorado State University. We thank R. Cohen, F. Scavone, H. Kimura, S. DiPietro, A. Ambrosio, L. Stargell, A. Thurston, and J. Chao for help with experiments. We thank Wu *et al.* (*25*) for sharing their preliminary data and the Transcription Imaging Consortium at the Janelia Research Campus of the Howard Hughes Medical Institute for creating the environment that made our interactions and discussions possible. T.M. and T.J.S. planned, analyzed, and carried out all experiments except for microinjections. T.J.S., T.M., and K.L. wrote the manuscript. K.L. helped with plasmid construction and transfections, cell culture, analysis, Western blotting, and figures. K.F.D. and J.G.D. performed microinjections. B.P.E. provided guidance for the multicolor single-molecule microscopy. Z.Z. purified Halo-MCP. L.L.L. and S.V. provided HA and FLAG SM constructs. L.D.L. and J.B.G. provided fluorophores. T.L. provided help with experimental design.

SUPPLEMENTARY MATERIALS

www.sciencemag.org/content/352/6292/1425/suppl/DC1
Materials and Methods
Supplementary Text
Figs. S1 to S12
References (*27*–*33*)
Movies S1 to S8

17 December 2015; accepted 28 April 2016
Published online 5 May 2016
10.1126/science.aaf0899

Science
AAAS

Real-time quantification of single RNA translation dynamics in living cells

Tatsuya Morisaki, Kenneth Lyon, Keith F. DeLuca, Jennifer G. DeLuca, Brian P. English, Zhengjian Zhang, Luke D. Lavis, Jonathan B. Grimm, Sarada Viswanathan, Loren L. Looger, Timothee Lionnet and Timothy J. Stasevich (May 5, 2016)
Science **352** (6292), 1425-1429. [doi: 10.1126/science.aaf0899]
originally published online May 5, 2016

Editor's Summary

The when, where, and how of translation

High-resolution single-molecule imaging shows the spatial and temporal dynamics of molecular events (see the Perspective by Iwasaki and Ingolia). Wu *et al.* and Morisaki *et al.* developed an approach to study the translation of single messenger RNAs (mRNAs) in live cells. Nascent polypeptides containing multimerized epitopes were imaged with fluorescent antibody fragments, while simultaneously detecting the single mRNAs using a different fluorescent tag. The approach enabled a direct readout of initiation and elongation, as well as revealing the spatial distribution of translation and allowing the correlation of polysome motility with translation dynamics. Membrane-targeted mRNAs could be distinguished from cytoplasmic mRNAs, as could single polysomes from higher-order polysomal complexes. Furthermore, the work reveals the stochasticity of translation, which can occur constitutively or in bursts, much like transcription, and the spatial regulation of translation in neuronal dendrites.

Science, this issue p. 1430, p. 1425; see also p. 1391

Science (print ISSN 0036-8075; online ISSN 1095-9203) is published weekly, except the last week in December, by the American Association for the Advancement of Science, 1200 New York Avenue NW, Washington, DC 20005.

www.sciencemag.org/cgi/content/full/science.aaf0899/DC1

Supplementary Materials for

Real-time quantification of single RNA translation dynamics in living cells

Tatsuya Morisaki, Kenneth Lyon, Keith F. DeLuca, Jennifer G. DeLuca, Brian P. English, Zhengjian Zhang, Luke D. Lavis, Jonathan B. Grimm, Sarada Viswanathan, Loren L. Looger, Timothee Lionnet, Timothy J. Stasevich*

*Corresponding author. Email: tim.stasevich@colostate.edu

Published 5 May 2016 on *Science* First Release
DOI: 10.1126/science.aaf0899

This PDF file includes:

Materials and Methods
Supplementary Text
Figs. S1 to S12
Full Reference List
Captions for Movies S1 to S8

Other Supplementary Material for this manuscript includes the following:
(available at www.sciencemag.org/cgi/content/full/science.aaf0899/DC1)

Movies S1 to S8

Materials and Methods

Plasmid Construction

The coding region of the spaghetti monster 10X FLAG-tag (SM) (5) was obtained by polymerase chain reaction (PCR) of a pCAG_mRuby2_smFP_FLAG (#59760, Addgene; mRuby2-based) template, using the following primers: 5'-GAG GAG GAG GCG GCC GCC ACC ATG GAC TAC AAG GAC GAC GAC GAC AAA GG-3'; 5'-CTC CTC CTC CTG CAG TGA ACC TCC TCC ACC TGA TCC ACC GCC TCC CTT ATC ATC ATC ATC CTT GTA ATC C-3'. The PCR product was flanked by NotI and PstI, and fused to the N terminal of beta-actin followed by the beta-actin zipcode and 24 MS2 stem loops in the 3' UTR (4) to obtain SM-beta-actin. The beta-actin coding region of SM-beta-actin was then digested out with PstI and NheI to construct SM-KDM5B and SM-H2B. For SM-KDM5B construction, the following oligo DNAs were annealed and inserted between PstI and NheI of digested SM-beta-actin to introduce AsiSI and PmeI sites: 5'-GGC GAT CGC CAT GGC CGT TTA AAC G-3'; 5'-CTA GCG TTT AAA CGG CCA TGG CGA TCG CCT GCA-3'. This product was then digested with AsiSI and PmeI, and replaced by the coding sequence of KDM5B acquired by digesting pFN21AAE9635 (Kazusa DNA Res. Inst.) with AsiSI and PmeI. For SM-H2B construction, the H2B coding region was PCR amplified from GFP-H2B (#11680, Addgene) using the following primers: 5'-GGG GCG GCC GCC ACC ATG CTG CAG CCA GAG CCA GCG AAG TCT GCT CCC G-3'; 5'- GGG GCT AGC CTA CAT ATG CTT AGC GCT GGT GTA CTT GGT GAT GGC CT-3'. The PCR product was flanked by PstI and NheI, and inserted between PstI and NheI of digested SM-beta-actin. HA-KDM5B was constructed via HA-beta-actin because of the availability of unique restriction enzyme sites. To obtain HA-beta-actin, the coding region of spaghetti monster 10X HA-tag was PCR amplified from pCAG_smFP_HA (#59759, Addgene, GFP-based) using the following primers: 5'- GGT TCG GCT TCT GGC GTG TGA CC-3'; 5'- CTC CTC CTC CTG CAG TGA ACC TCC TCC ACC TGA TCC ACC GCC TCC AGC GTA GTC CGG GAC ATC GTA CGG GTA ACC G-3' and replaced into the coding region of 10X FLAG-tag of SM-beta-actin by using NotI and PstI. The beta-actin coding region was then replaced with the KDM5B coding region to construct HA-KDM5B following the same manner described above.

Fab Generation and Dye-Conjugation

Pierce mouse IgG1 preparation kit (Thermo Scientific) was used to generate Fab according to the manufacturer's instruction. Briefly, immobilized ficin in the presence of 25 mM cysteine was used to digest FLAG (Wako, 012-22384 Anti DYKDDDDK mouse IgG2b monoclonal) and HA (Sigma-Aldrich, H3663 HA-7 mouse IgG1 monoclonal; required clean-up with NAb Protein A column (Thermo Scientific)) antibodies to create Fab. Fab were separated from the Fc region using NAb Protein A column. After elution Fab were concentrated to 1 mg/ml and conjugated to either Alexa Fluor 488 (Alexa488) or Cy3. Alexa488 tetrafluorophenyl ester (Invitrogen) or Cy3 N-hydroxysuccinimide ester (Invitrogen) were dissolved in DMSO and stored at -20°C. 100 µg of Fab were diluted into 100 µl of 100 mM $NaHCO_3$ (pH 8.5). 1.33 µl of Cy3 or 5.33 µl Alexa488 was added to this solution and incubated with end-over-end rotation for 1-2 hours at room

temperature. The conjugated Fab were then eluted from a PBS pre-equilibrated PD-mini G-25 desalting column (GE Healthcare) that removed unconjugated dye. Conjugated Fabs were then concentrated using an Ultrafree 0.5 filter (10k-cut off; Millipore) to 1 mg/ml. The Fab:dye ratio was calculated using the absorbance at 280 and 495 or 550 nm, and using the extinction coefficient of Fab with the dye correction factor at 280 nm provided by the manufacturers (0.11 or 0.08 for Alexa488 and Cy3, respectively). The degree of labeling was calculated using the following formula:

$$(DOL) = \left(\frac{\varepsilon protein}{\varepsilon dye}\right)\left(\frac{1}{1/_{Aratio,measured} - CF}\right) \quad (1)$$

Only Fab with a DOL of ~1 were used in experiments.

MCP Purification

His-tagged MCP was purified with Ni-NTA-agarose (Qiagen) following the manufacturer's instructions with minor modifications. Briefly, the bacteria were lysed in a PBS-based buffer containing a complete set of protease inhibitors (Roche), binding to the Ni-NTA resin was carried out in the presence of 10 mM imidazole. After washing with 20 and 50 mM imidazole in PBS, the protein was eluted with 300 mM imidazole in PBS, and directly used for experiments. The rest was dialyzed against a HEPES-based buffer (10% glycerol, 25 mM HEPES pH 7.9, 12.5 mM $MgCl_2$, 100 mM KCl, 0.1 mM EDTA, 0.01 % NP-40 detergent, and 1 mM DTT) and stored at -80 °C after snap-freezing by liquid nitrogen.

Cell Culture, Transfection, and Bead-Loading

U2OS cells were grown in DMEM (Thermo Scientific) supplemented with 10% (v/v) FBS, 1 mM L-glutamine and 1% (v/v) Penicillin-streptomycin. Prior to experiments, cells were plated into a 35 mm MatTek chamber (MatTek) and transiently transfected using Lipofectamine 3000 (Thermo Scientific) according to the manufacturer's instructions. 2-3 hours after transfection, cells were bead-loaded with fluorescently labeled Fab and purified MCP-HaloTag protein as previously described (27, 28). Briefly, 100 μg/ml of fluorescently labeled Fab and 33 μg/ml of purified MCP-HaloTag protein were prepared in 4 μl of PBS. After removing DMEM, this 4 μl solution was pipetted on top of the cells and ~106 μm glass beads (Sigma Aldrich) were then evenly distributed over the cells. The chamber was then tapped firmly 6 times, and DMEM was added back to the cells. 2 hours after bead-loading, the cells were washed three times with phenol-red-free complete DMEM to remove glass beads, and 200 nM of JF646-HaloTag ligand (a cell permeable fluorogenic ligand (7)) was added to label MCP-HaloTag protein. After 30 min of incubation, the cells were washed three times with phenol-red-free complete DMEM to remove the unliganded fluorophores. Cells were immediately imaged for translation experiments, whereas cells were incubated an additional 18 hours before imaging for testing localization of constructs and SM-H2B FRAP experiments.

Single Molecule Tracking Microscopy

To track single molecule mRNA translation events, we used a custom-built widefield fluorescence microscope with a highly inclined illumination scheme (29) based on a previously described design (30). Briefly, the excitation beams, 488, 561 and 637 nm solid-state lasers (Vortran), were coupled and focused on the back focal plane of the objective (60X, NA 1.49 oil immersion objective, Olympus). The emission signals were split by an imaging grade, ultra-flat dichroic mirror (T660lpxr, Chroma) and detected by two aligned EM-CCD (iXon Ultra 888, Andor) cameras by focusing with 300 mm tube lenses (this lens combination produces 100X images with 130 nm/pixel). Live cells were placed into a custom-built incubation chamber at 37 °C and 5% CO_2 on a piezoelectric stage (PZU-2150, Applied Scientific Instrumentation). The focus was maintained with the CRISP Autofocus System (CRISP-890, Applied Scientific Instrumentation). The lasers, the cameras, and the piezoelectric stage were synchronized by an Arduino UNO board (Arduino). Image acquisition was performed using open source Micro-Manager software (31). For two-color single molecule tracking, the far-red signal from mRNA visualized with MCP-Halo-JF646 and the red signal from elongating protein visualized with Cy3-FLAG-Fab were simultaneously imaged by the two cameras without any time delay. Note that all colors we describe in the text and we show in the figures are based on the color of excitation lasers, namely mRNA in red (JF646) and protein in green (Cy3). Imaging size was set to 512 x 512 pixels2 (66.6 x 66.6 μm^2), and exposure time was selected as 53.64 msec. The readout time of the cameras from the combination of our imaging size and the vertical shift speed we selected was 23.36 msec, resulting in our imaging rate of 13 Hz (70 msec per image). The excitation laser lines were digitally synched such that they illuminate the cells only when the camera is exposing in order to avoid any excess observational photobleaching. To capture the whole thickness of the cytoplasm of U2OS cells, 13 z-stack of step size 500 nm (6 µm in total) were imaged using the piezoelectric stage, resulting in our total cellular imaging rate of 1 Hz (1 sec per volume). Laser power was set to 160 µW and 340 µW at the back focal plane of the objective for 561 nm and 637 nm, respectively, throughout experiments. With this relatively weaker laser power setting, only signal from more than one SM could be detected which allowed us to (1) avoid detecting already translated single protein products, (2) image only polysomes, and (3) reduce excess observational photobleaching. For single-FLAG experiments were performed with 1.5 mW of 561 nm to visualize single fluorophore molecules. KDM5B fluorescence correlation spectroscopy (FCS) experiments were carried out with 50 µW and 170 µW of 561 nm and 637 nm, respectively (this was possible because KDM5B polysomes are relatively bright).

For three-color experiments, the far-red signal of mRNA was imaged on one camera, and the red and the green signal of proteins visualized by Cy3-FLAG-Fab and Alexa488-HA-Fab, respectively, were imaged on the other camera. Note again that all colors described in the text and figures are based on the color of excitation lasers as mentioned above, namely mRNA in red (JF646), FLAG-protein in green (Cy3), and HA-protein in blue (Alexa488). Image acquisitions were performed with the same conditions described above, except that an additional 70 µW of 488 nm laser was used to excite Alexa488, and that Cy3 and Alexa488 signals were imaged alternatively. For this, the piezoelectric stage was moved to the next position every 2 images (Cy3 and Alexa488),

resulting in our imaging rate of 0.5 Hz (2 sec per volume in 3 color). With these settings, there was only a 77 msec time delay between the alternating Cy3 and Alexa488 image acquisitions.

Particle Tracking

Collected images were first pre-processed with Fiji (32). Briefly, the 3D images were projected to 2D images by a maximum intensity projection, background subtracted, and corrected for observational photobleaching (using the built-in Bleach Correction tool). Pre-processed images were then analyzed by a custom-written *Mathematica* (Wolfram Research) routine to detect and track particles. Specifically, 3-frame rolling average movies were created and the averaged images were processed with a band-pass filter to accentuate particles so their positions could be detected using an appropriate threshold intensity value. Detected particles were linked through time by allowing a maximum displacement between consecutive frames of 3 pixels corresponding to 390 nm in length. Tracks lasting at least 25 seconds were selected and the precise coordinates and intensity of each particle were determined by fitting (using the built-in *Mathematica* routine NonlinearModelFit) the original, pre-processed images to 2D Gaussians of the following form:

$$I(x,y) = I_{BG} + Ie^{-\frac{(x-x0)^2}{2\sigma_x^2} - \frac{(y-y0)^2}{2\sigma_y^2}}, \quad (2)$$

where I_{BG} is the background fluorescence, I the particle intensity, and (x_0, y_0) the particle location. For fitting, σ_x and σ_y were fixed at $\sigma_x = \sigma_y = 1.5$ pixels (195 nm), values determined by fitting diffraction limited spots acquired from images of 200 nm diameter beads (Tetraspeck, Molecular Probes/Thermo-Fisher) taken with the same imaging conditions. Fitted parameters were saved for each track for further analysis, along with 95% confidence intervals of the fitted parameters. The offset between the two cameras was registered using the built-in *Mathematica* routine FindGeometricTransform to find the transform function that best aligned the fitted positions of 200 nm diameter Tetraspeck beads evenly spread out across the image field-of-view. Note that we did not register the images, but only the fitted positions in order to avoid introducing any distortion into images. This is why a slight offset can be observed between the red and the green particles even though they are supposed to be in the same diffraction limited spots from our calculations. The only exceptions being the mRNA-centered cropped images showing particles in Fig. 1F, 4D and Sup. Fig. 12, where the protein image has been corrected by the transformation function. The *Mathematica* source code for tracking particles is available upon request.

Puromycin Treatment

Cells transiently-transfected with SM-KDM5B, bead-loaded with Cy3-conjugated α-FLAG Fab and MCP-HaloTag protein (labeled with JF646-HaloTag ligand) were imaged as described above, except that a 6.5 second interval was introduced every 13 frames (every one volume). After acquiring 10 time points of pre-treatment images, cells were treated with a final concentration of 50 μg/ml puromycin. After treatment, the cells were imaged under the same settings used for the pre-treatment imaging. For the control, the same experiments were performed except that the cells were treated with the vehicle of

puromycin (H_2O). The number of detected polysomes (co-moving SM-KDM5B and mRNA labeled by Fab and MCP, respectively) was then normalized by the average number of polysomes detected during pre-treatment and plotted as a function of time.

Micro-Injection

Cy3 conjugated α-FLAG Fab were micro-injected into cells transiently-transfected with SM-KDM5B, bead-loaded with MCP-HaloTag protein alone (without Fab), and labeled with JF646-HaloTag ligand. Fab was diluted into Injection Buffer (IB: 10 mM Na_2HPO_4, pH 7.4, 100 mM KCl, and 1 mM MgCl2) and loaded into a final needle concentration of 0.1 mg/ml (Eppendorf, Femtotips II). Transiently-transfected and bead-loaded cells were identified by their characteristic MCP punctae in the far-red channel. These were then micro-injected with a FemtoJet II Injector (Eppendorf) on an inverted Nikon TE-2000 microscope equipped with a 100X, NA 1.42 oil immersion objective (Nikon) and a Photometrics HQ2 camera (Roper Scientific) after acquiring a pre-injecting image. Immediately after the injection, two-color (543 nm and 646 nm) time-lapse imaging (at 1 Hz) was manually started. The earliest time point achievable was ~3 seconds after the injection.

Fluorescence Recovery After Photobleaching (FRAP)

For examination of k_{off} of Cy3-FLAG-Fab, FRAP experiments were performed on cells transiently transfected with SM-H2B and bead-loaded with Cy3 conjugated α-FLAG Fab using a Zeiss LSM 880 confocal microscope equipped with a 63X, NA 1.40 oil immersion objective (Carl Zeiss). After acquiring 5 pre-bleach images (265 x 256 pixels^2; pixel size = 263 nm) every 5 seconds, half of the nucleus was photobleached using 100% 561 nm laser illumination. The fluorescence recovery in the photobleached region was then monitored for 50 frames under the same settings used for pre-bleach imaging. Cell movement was corrected using the StackReg ImageJ plugin (33). After subtracting background and correcting for observational photobleaching, the average fluorescence intensity in the photobleached region was plotted as a function of time.

For examination of translation elongation, FRAP on SM-KDM5B polysomes was performed on the LSM880. Cells transiently-transfected with SM-KDM5B and bead-loaded with Cy3-conjugated α-FLAG Fab and MCP-HaloTag protein (labeled with JF646-HaloTag ligand) were imaged every 12.8 sec in z-stacks containing 10 planes with a step size of 500 nm (265 x 256 pixels^2; voxel size = 166 x 166 x 500 nm). After acquiring 5 pre-bleach images, a fraction of the cytoplasm containing several translation sites was photobleached using 561 nm laser illumination, such that only the signal from Fab was photobleached, not mRNA. Subsequently cells were imaged for 30 frames (6.4 min) with the same settings used for pre-bleach imaging. Collected 3D images were then projected to 2D images by a maximum intensity projection. Translation sites were tracked manually following the mRNA signals and the fluorescence intensity of Cy3 was measured. The control translation sites that were not photobleached were also tracked, and their Cy3 intensities were used to correct observational photobleaching. This introduced some additional noise into our measurement, making it difficult to precisely determine the full recovery time. To approximate this time, we averaged the photobleach corrected curves and fit with a single exponential to estimate the 80% and 90% recovery times.

Fluorescence Correlation Spectroscopy (FCS)

SM-H2B, SM-beta-actin, and SM-KDM5B were transfected into cells that were subsequently bead loaded 3 hours later with MCP-HaloTag (labeled with JF646-HaloTag ligand) and Cy3-conjugated α-FLAG Fab. 3-6 hours after bead-loading, single polysomes were imaged in two colors (mRNA and protein) and tracked for 300 time points total at 1, 1/3, or 1/10 Hz, respectively, as described above. The mRNA intensity signal was stable and relatively easy to track, so its position was used as a starting guess for fitting the protein signal with a Gaussian. This allowed us to measure protein intensity in polysomes even if the intensity dropped below background levels. This resulted in an intensity time series that was stored for each tracked polysome. These were processed individually as follows: First, any detectable decay in polysome intensity due to unintentional photobleaching while imaging was corrected for by dividing out fits to an exponential decay. This yielded a new intensity time series $I(t)$ without decay that was re-normalized to the average intensity of the original time series and stored. Second, the intensity fluctuations about the average intensity $\delta I(t)$ were also stored. Third, the auto-correlation curves $G(\tau)$ were generated from these time series using the following formula:

$$G(\tau) = \frac{\langle \delta I(t) \delta I(t+\tau) \rangle}{\langle I(t) \rangle^2}, \quad (3)$$

where the brackets represent an average of the time series data over the discrete time points t in the time series and τ is a discrete time shift in units of the discrete t (using the built-in *Mathematica* function ListCorrelate). Fourth, for fitting, data was binned so as not to overweight the end of the autocorrelation compared to the beginning (where most of the change occurs). Specifically, the first 8 data points in $G(\tau)$ were not binned, points 9-24 were in bins of length two (i.e. (9,10), (11,12), (13,14), …, (23,24)), time points 25-56 were in bins of length four (i.e. ((25,26,27,28), (29,30,31,32), …, (53,54,55,66)), time points 57-120 were in bins of length 8 (i.e. (57, 58, 59, 60, 61, 62, 63, 64), (65, 66, 67, 68, 69, 70, 71, 72), … (113, 114, 115, 116, 117, 118, 119, 120)), and so on. The average value of τ and $G(\tau)$ in each bin was calculated and stored for subsequent fitting.

To fit the elongation dwell time T (the average time it takes a ribosome to translate the protein) from the measured auto-correlation, the following formula was applied (12):

$$G(\tau) = \frac{(T-\tau)}{cT^2} H(T-\tau) \, , \quad (4)$$

where c is the translation initiation rate and $H(t)$ is the Heaviside step function equal to 1 for $t > 0$ and zero otherwise. This is an approximation of the exact correlation function that was derived in (12) to describe MCP intensity fluctuations due to transcription at a gene with repeated MS2 stem loops in the 5' UTR. The approximation is valid when the gene is long compared to the MS2 stem loop tag. Due to the analogies between our Fab-based peptide labeling system and the MS2-based RNA labeling system and between transcription and translation, the model is directly applicable to our experimental data. For shorter proteins, like H2B, the approximation is not as good because translation of the epitopes in the tag contribute more to $G(\tau)$. Nevertheless, fits still provide a reasonable upper bound on the elongation dwell time. Fitting was performed with

Mathematica using the built-in function NonlinearModelFit. Error bars show the 95% confidence intervals.

Western Blots

U2OS cells were transiently transfected with SM-H2B, SM-beta-actin, and SM-KDM5B, and were lysed in RIPA buffer with cOmplete Protease Inhibitor (Roche). The protein concentration was then measured using a BCA protein assay kit (Pierce). 5 µg of total protein was loaded on a 12.5% (for SM-H2B and SM-beta-actin) or 7.5% (for SM-KDM5B) acrylamide Tris-Glycine gel and run for 15 minutes at 75 V through a stacking gel and for 1 hour and 40 minutes at 125 V through a resolving gel. Proteins were then transferred to a PVDF membrane (Invitrogen) and stained for 1 hour at room temperature with α-FLAG mouse antibody (1:5,000, 1E6, Wako). HRP-donkey α-mouse IgG (1:10,000, Jackson Immuno Research) was used as a secondary antibody. The protein of interest was then detected using ECL Prime (GE Healthcare).

Polysome Profiling

U2OS cells were cultured in a 150-mm dish and were transiently transfected with SM-beta-actin and SM-KDM5B. 6 or 24 hours after transfection, cells were incubated with fresh DMEM supplemented with 100 µg/ml cycloheximide for 10 minutes to immobilize mRNAs on ribosomes. Cells were then washed twice with ice cold PBS supplemented with 100 µg/ml cycloheximide, and harvested by scraping followed by centrifugation. Cell pellets were resuspended with ice cold lysis buffer (20 mM HEPES 7.4 pH, 150 mM KCl, 15 mM $MgCl_2$, 2% NP-40, 1 mM DTT, cOmplete Protease Inhibitor (Roche), 4 U/ml RiboLock RNase Inhibitor (ThermoFisher), and 100 µg/ml cycloheximide) and incubated on ice for 5 minutes. Lysates were centrifuged at 13,000 g for 10 min at 4 °C, and the supernatant was loaded on 10-50% sucrose gradient (20 mM HEPES 7.4 pH, 150 mM KCl, 15 mM $MgCl_2$, 1 mM DTT, and 100 µg/ml cycloheximide) prepared with a Gradient Master (Biocomp Instruments). The sucrose gradient was centrifuged at 36,000 rpm for 3 hours at 4 °C with an SW 41 Ti rotor (Beckman Coulter). 100 µl fractions were successively taken from the top with a pipette in a cold room, after which absorbance at 260 nm was measured. Five consecutive fractions were then combined, and mixed with 1 ml of Trizol (Ambion) to purify RNA following the manufacture's instruction. The isolated total RNA were further purified using an RNeasy mini kit (Qiagen), and then reverse transcribed to cDNA using an iScript Select cDNA Synthesis Kit (Bio-Rad). The relative amount of SM-beta-actin and SM-KDM5B mRNA in each fraction was quantified by real-time qPCR on a CFX96 (Bio-Rad) using SYBR green chemistry with the following primer set which bind to MS2 stem loops: 5'-CCT CAA ACC TCT TCC CAC AA-3'; 5'-GTT GCT GAA CGG TTT GGT TT-3'.

Stochastic Monte Carlo simulations of live-cell translation experiments

Custom *Mathematica* code was written to simulate the experimentally measured fluctuations of fluorescence from polysomes containing SM-KDM5B mRNA transcripts. The time step of the simulation was chosen to be 10 ms and the total simulation time was set to 5000 s. The ribosome initiation and elongation rates were set to 1/30 s^{-1} and 10 aa/s, respectively. The probability of initiation and elongation (extension by one amino

acid) in a single 10 ms time step was therefore 1/3000 and 1/10, respectively. The N-terminal spaghetti monster tag was simulated such that a single α-FLAG Fab binds it when precisely 27, 235, and 325 amino acids of the tag are translated by a ribosome (this was done to mimic the three concentrated pockets of three to four FLAG epitopes in the spaghetti monster). At each time step, a random number between 0 and 1 was generated to test if a new ribosome initiates. As well, random numbers were generated for each elongating ribosome to test if they extend by a single amino acid. At each time step, the position of all bound ribosomes was recorded to calculate the total fluorescence. If ribosomes extended the length of the protein coding region of the transcript, they escaped with probability 1. Simulations were equilibrated for a 1000 s before fluorescence was recorded. To simulate 100 μg/ml cycloheximide treatment, the probabilities of initiation and elongation were made time-dependent such that they decayed to zero in 3000 and 2000 seconds (after the equilibration), respectively. Movies S6 and S7 show sample simulation movies of normal and cycloheximide-stalled translation. All code is available upon request.

Supplementary Text

Supplementary Calculation

Derivation of analytic formulas for the probability of polysome formation (frequency of polysomes) and the number of ribosomes per polysome

Assume ribosomes initiate randomly on mRNA such that on average a ribosome will translate n amino acids before another ribosome initiates. To calculate the probability of finding M ribosomes on an mRNA encoding a protein with N amino acids total, we make the analogy to rolling M sixes in N die tosses ($N > M$). Here, the probability of a six is $p = 1/6$, while the probability of anything other than a six is $q = 5/6$. Then, the probability of exactly M sixes in N tosses is

$$P(M, N, n) = \binom{N}{M} p^M q^{N-M} \tag{S.1}$$

By analogy, the probability P_{rib} of finding M ribosomes on an mRNA encoding N amino acids is

$$P_{rib}(M, N, n) = \binom{N}{M} \left(\frac{1}{n}\right)^M \left(\frac{n-1}{n}\right)^{N-M} \tag{S.2}$$

Here $p = 1/n$, which is the probability of initiation in the time it takes a ribosome to translate one amino acid, i.e. the ratio of the ribosome initiation rate to the elongation rate. Thus, to take the analogy further, every time a ribosome translates one amino acid, it is as if there is a coin toss as to whether or not another ribosome will initiate. In total, there will be N coin tosses before the ribosome terminates, one for each amino acid the mRNA encodes.

The average number of ribosomes per mRNA is then:

$$\langle M \rangle = \sum_{M=0}^{\infty} M \binom{N}{M} \left(\frac{1}{n}\right)^{M} \left(\frac{n-1}{n}\right)^{N-M} = \frac{N}{n} = Np. \quad \text{(S.3)}$$

In other words, the longer the protein (of length N), the more ribosomes. If the average number of ribosomes is plotted as a function of protein length (N), then the slope will give the ratio of the initiation rate to the elongation rate.

The probability P_{poly} to find a polysome (an mRNA with two or more ribosomes translating) can now be calculated as follows

$$P_{poly}(N, n) = 1 - P_{rib}(0, N, n) - P_{rib}(1, N, n) \quad \text{(S.4)}$$

This gives the frequency that polysomes are observed. Similarly, the average number of ribosomes per polysome N_{poly} can be calculated as

$$N_{poly}(N, n) = \frac{1}{P_{poly}(N, n)} \sum_{M=2}^{\infty} M\, P_{rib}(M, N, n) \quad \text{(S.5)}$$

Here the pre-factor just normalizes the probabilities in the sum to add up to one (since we are restricting our attention to polysomes).

According to our measurements, there are 5.1 ± 0.9 ribosomes per KDM5B polysome. Since KDM5B polysomes represented the vast majority of mRNA (86 ± 2%), simply dividing the length of KDM5B (1544 amino acids) by 5.1 provides a good estimate for how many amino acids a ribosome translates before another initiates: 1544/(5.1 ± 0.9) = 303 ± 53 amino acids (error is SEM). We can now use this number to calculate the expected frequency of polysomes:

$$P_{poly}^{KDM5B} \equiv P_{poly}(N = 1544, n = 303 \pm 53) = 96.3 \pm 3\% \quad \text{(S.6)}$$

In other words, there is a less than 5% chance that a KDM5B mRNA will be loaded with fewer than 2 ribosomes. This is close to the frequency of polysomes we measured.

Now, if we further assume that H2B and beta-actin have the same elongation and initiation rates as KDM5B (i.e. same $n = 303 \pm 53$), then we can calculate the expected frequency of polysomes:

$$P_{poly}^{\beta-actin} \equiv P_{poly}(N = 374, n = 303 \pm 53) = 35\ \pm 9\% \quad \text{(S.7)}$$

$$P_{poly}^{H2B} \equiv P_{poly}(N = 125, n = 303 \pm 53) = 6.5 \pm 3\% \quad \text{(S.8)}$$

Likewise, we can calculate the average number of ribosomes per polysome:

$$N_{poly}^{\beta-actin} \equiv N_{poly}(N = 374, n = 303 \pm 53) = 2.5 \pm 0.1 \quad \text{(S.9)}$$

$$N_{poly}^{H2B} \equiv N_{poly}(N = 125, n = 303 \pm 53) = 2.15 \pm 0.04 \quad \text{(S.10)}$$

These are also reasonably close to what we measured (19 ± 4% of beta-actin mRNA containing 3.1 ± 0.5 ribosomes and 4 ± 1% of H2B mRNA containing 2.1 ± 0.4 ribosomes), confirming our estimate of $n = 303 \pm 53$ and suggesting KDM5B, beta-actin, and H2B polysomes have similar initiation and elongation kinetics.

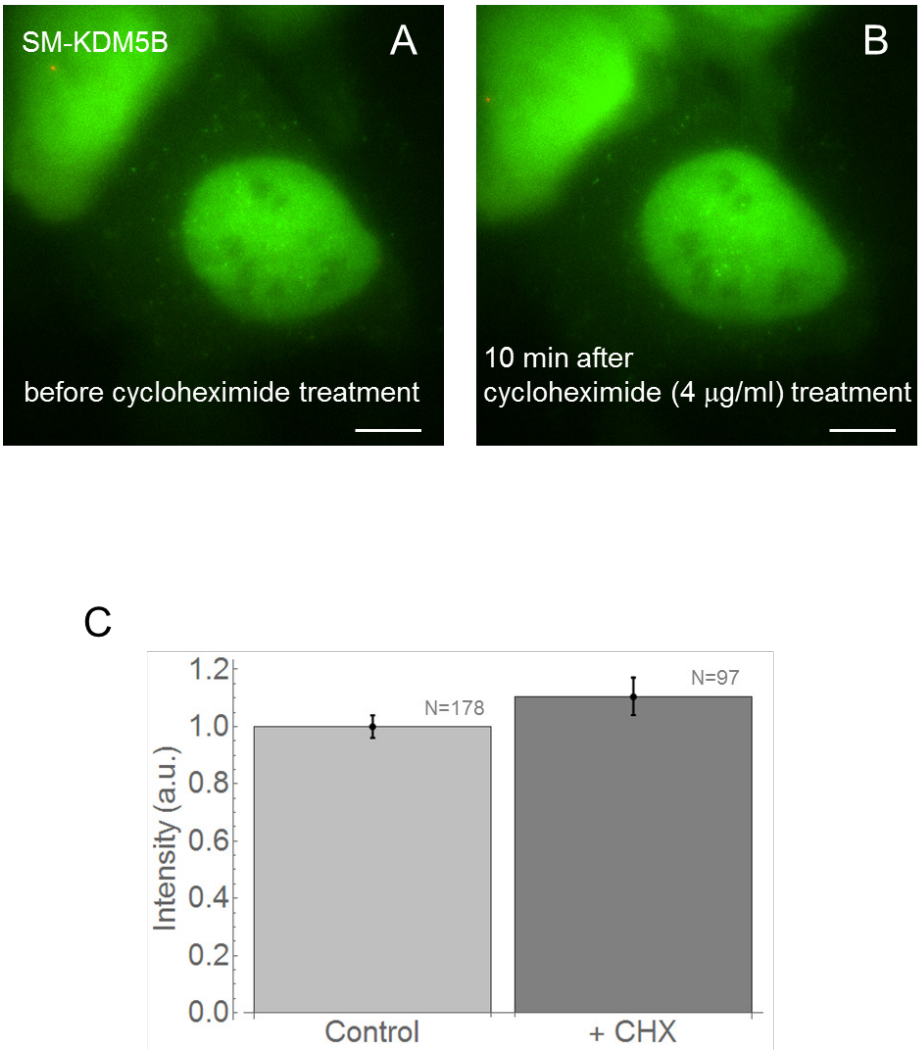

Fig. S1.

Cells expressing KDM5B-SM were treated with 4 µg/ml cycloheximide to slow elongation and load up more ribosomes. Polysomes in cells **A** before and **B** ten minutes after cycloheximide treatment. Cells after treatment were brighter than those before treatment, as quantified in **C**. Error bars show SEM. Scale bar, 10 µm.

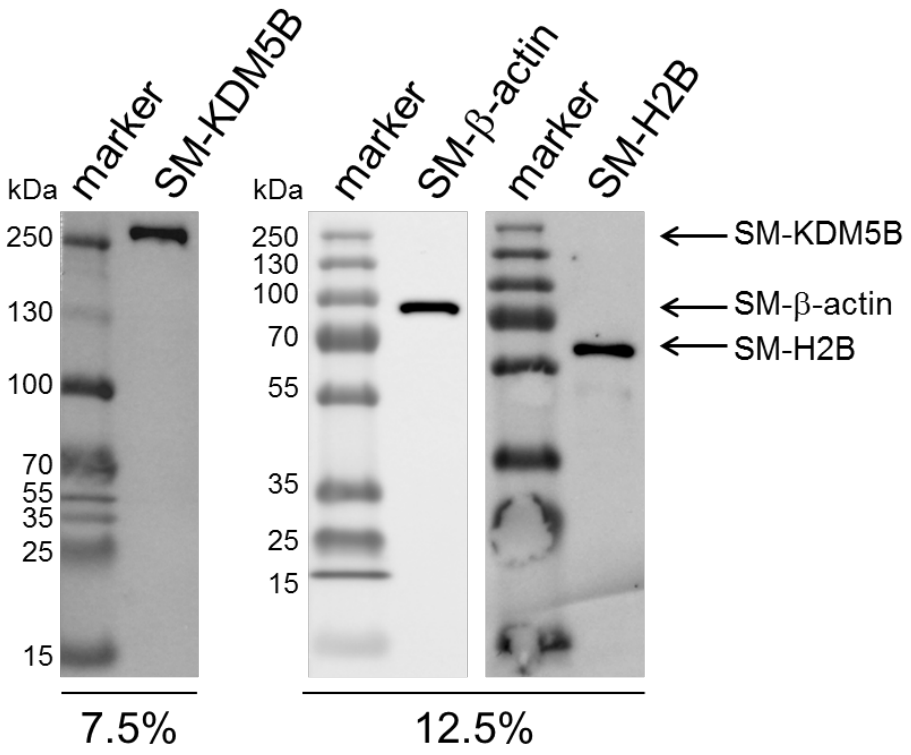

Fig. S2

Western blot analysis of SM-tagged constructs. From left to right, SM-KDM5B, SM-beta-actin, and SM-H2B. SM-tagged constructs are around their expected sizes, demonstrating the SM tag does not interfere with protein synthesis.

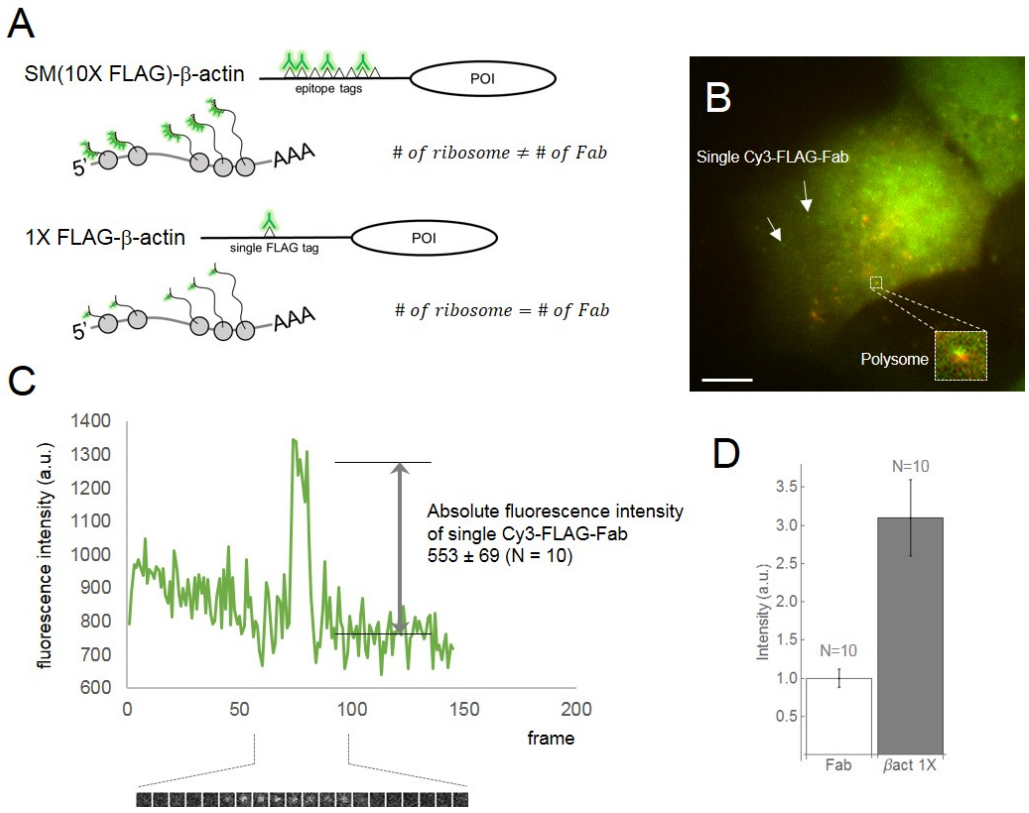

Fig. S3

A Schematic showing a 1X FLAG tag construct (bottom) designed to estimate the number of ribosomes (gray circles) per polysome since only one Fab (green "Y" shapes) can bind per ribosome. This provides a lower-bound estimate for the number of ribosomes because the single FLAG sites may not be saturated by Fab. **B** When the 1X FLAG plasmid is transfected into cells bead-loaded with MCP (red, for labeling mRNA) and Fab (green, for labeling the 1X FLAG tag) and imaged at high laser powers, single Fab could be seen alongside polysomes (marked by arrows). **C** A representative time series showing the intensity of a single detected Fab through time. The Fab photobleached in one step, indicating a single fluorophore. The height of the signal above background was used to calculate the average single Fab intensity. At bottom are images of the single Fab fluorescence shown in the time series. **D** The average single Fab intensity (white bar) compared to polysome intensity (gray bar) reveals approximately 3.1 ± 0.5 Fab per beta-actin polysome, indicating 3.1 ± 0.5 ribosomes per polysome. Data are normalized to signal from single Fab. Error bars show SEM. Scale bar, 10 µm.

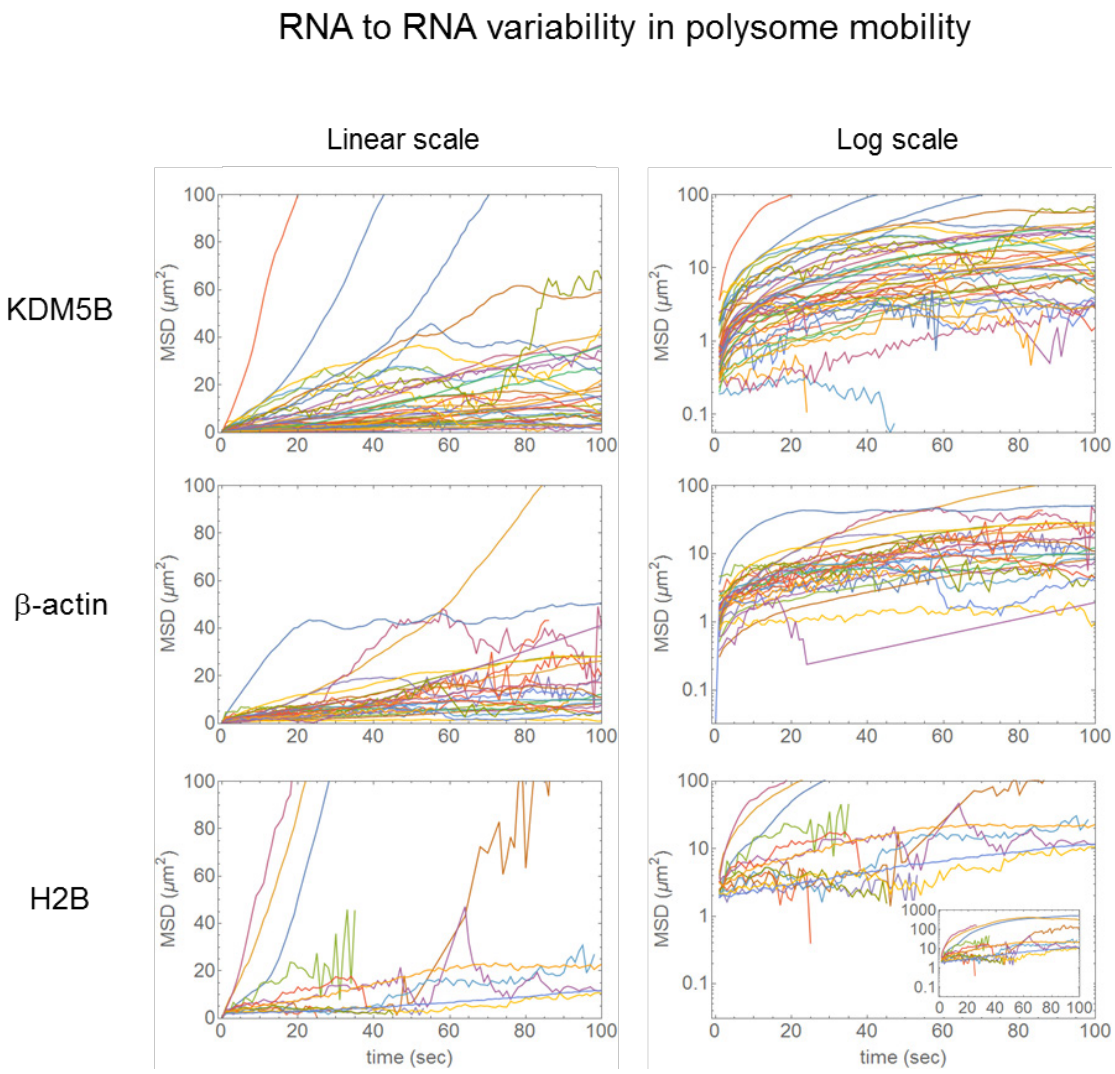

Fig. S4

Plots of the mean squared displacement (MSD) of single translating mRNA versus time (on linear and log scales) reveal significant variability in the mobility from mRNA to mRNA (different tracks in different colors). The variability is so great that based on mobility alone it can be difficult to distinguish a single KDM5B polysome from a beta-actin or H2B polysome.

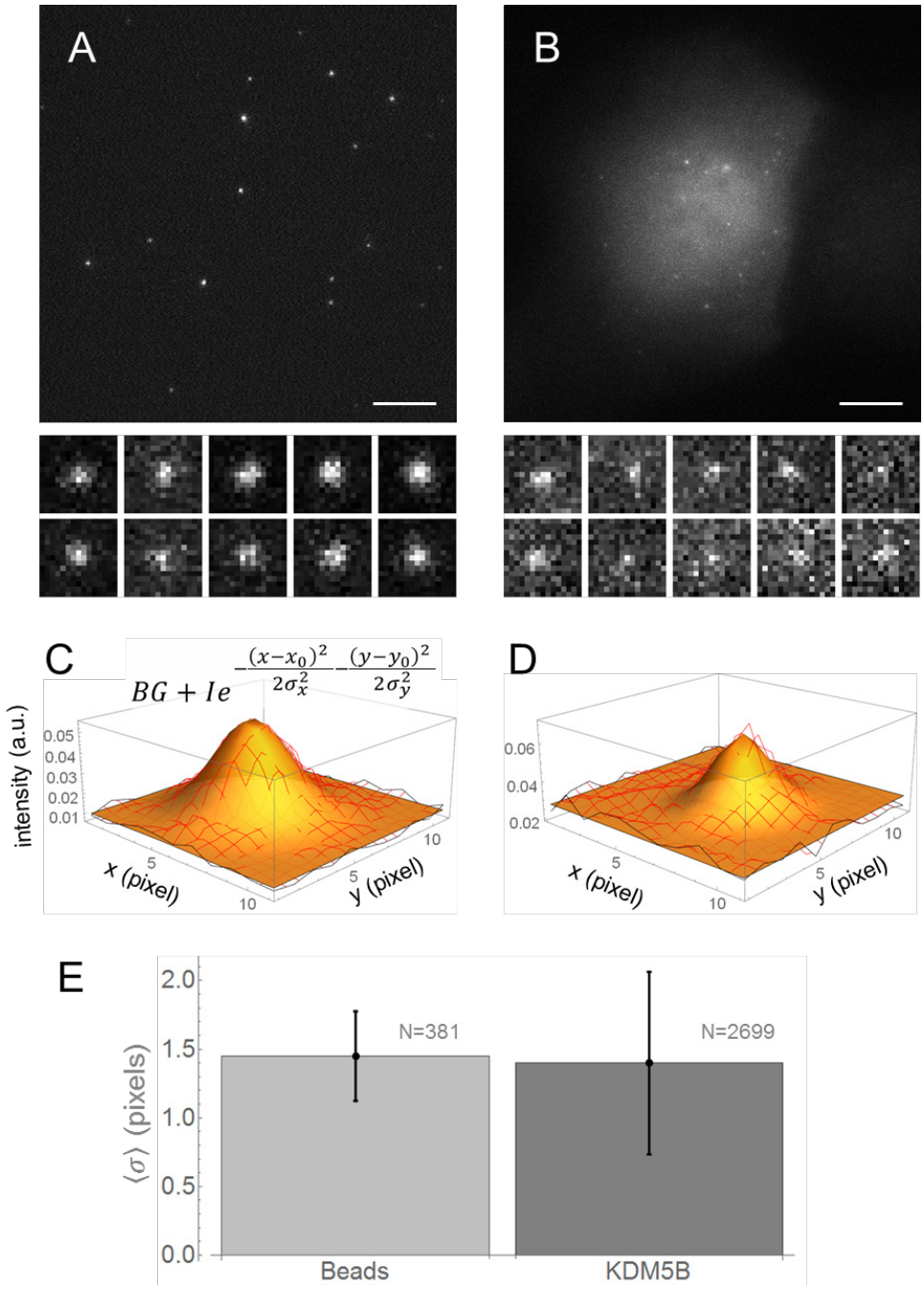

Fig. S5

A Diffraction limited images of 200 nm beads in comparison to images of SM-KDM5B polysomes. Sample 1.9 x 1.9 μm^2 images of individual beads and polysomes are shown below. Sample fits of beads **C** and polysomes **D** to Gaussians yield nearly identical average width $\langle\sigma\rangle \equiv \langle\sigma_x + \sigma_y\rangle/2$, as quantified in **E**. Here (x_0, y_0) is the center of the Gaussian, σ_x and σ_y are the widths of the Gaussian, I is the amplitude of the fluorescence intensity, and BG is the background fluorescence. Error bars show SD. Scale bar, 10 μm.

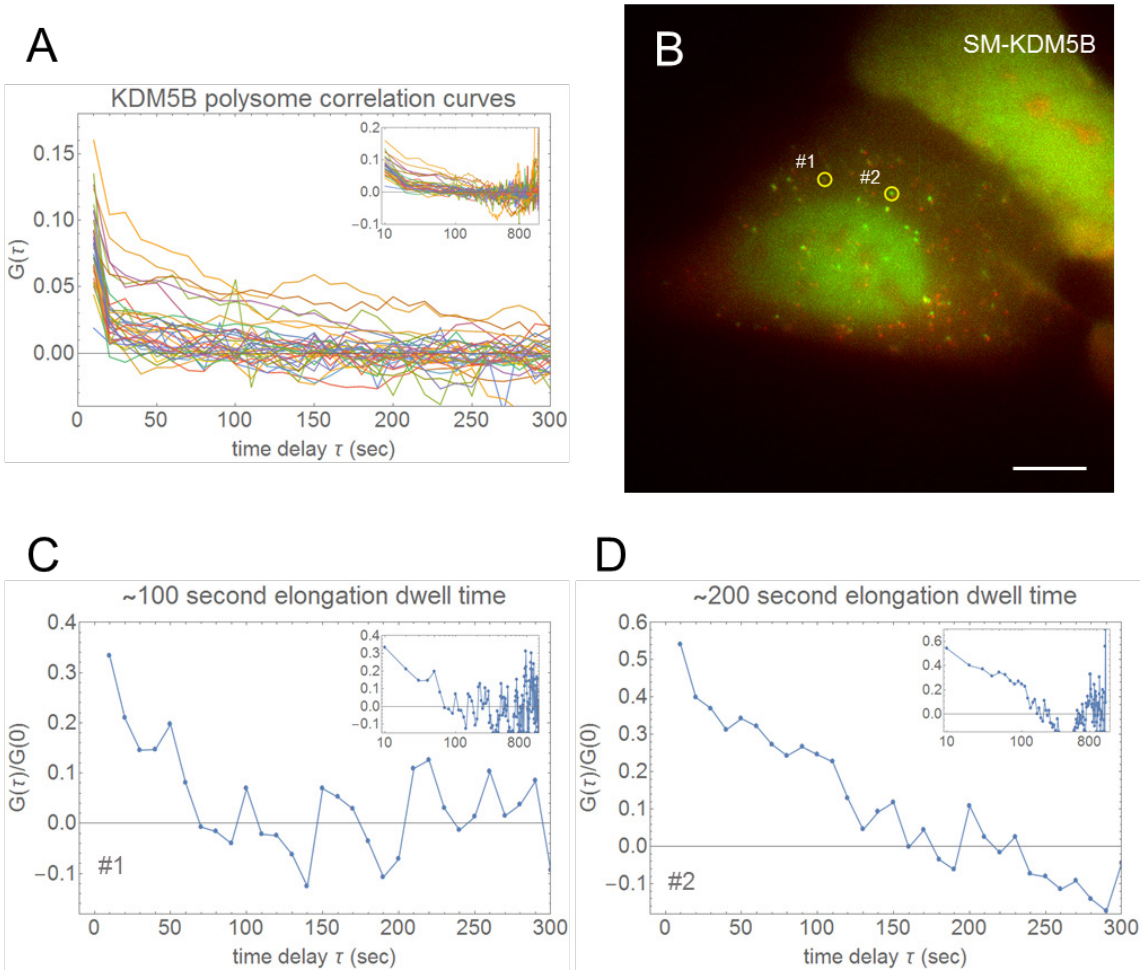

Fig. S6

A Example autocorrelation curves from single SM-KDM5B polysomes in the cell depicted in **B** showing the variability in translation dynamics. **C** The autocorrelation curve $G(\tau)$ corresponding to the polysome circled in B and labeled #1. The inset shows a log-scale version. The autocorrelation linearly drops to zero in ~100 sec, which would correspond to a faster than average elongation rate of ~15 amino acids per second. **D** The same as C, but now for the polysome in B labeled #2. The autocorrelation linearly drops to zero in ~200 sec, which would correspond to a slower than average elongation rate of ~8 amino acids per second. Scale bar, 10 µm. Note this cell is also shown in Sup. Movie 2 (imaged at 1 frame per minute compared to the 1 frame per 10 seconds used to generate this data).

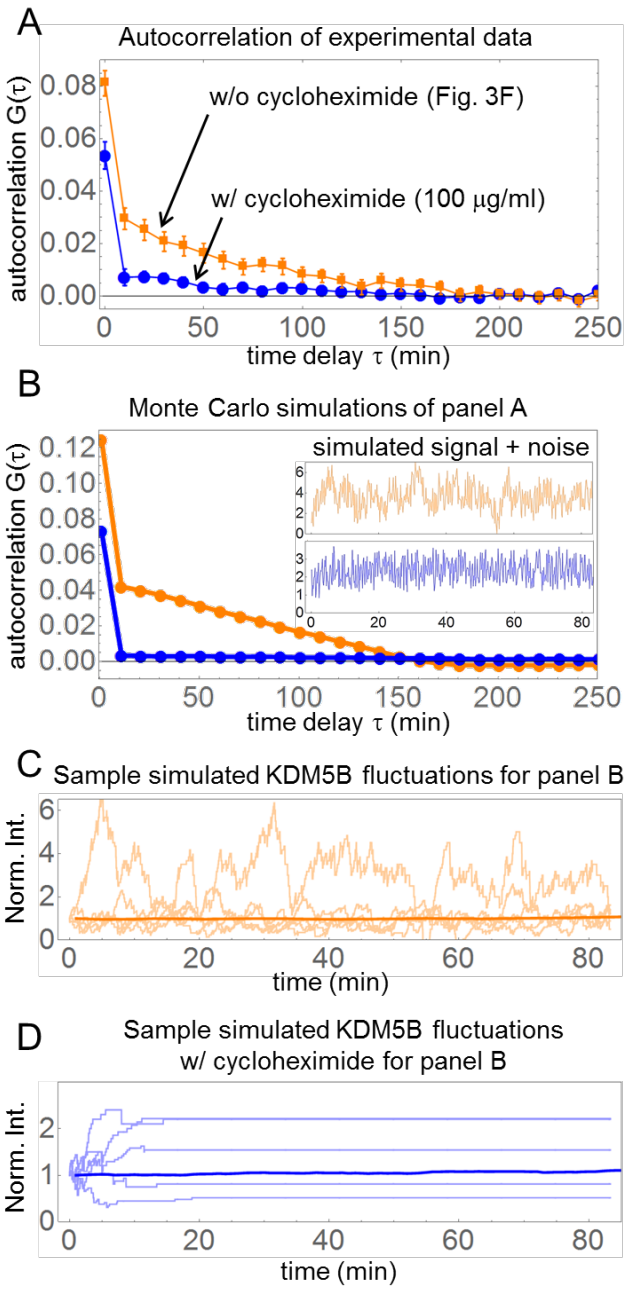

Fig. S7

Cells expressing KDM5B-SM were treated with 100 µg/ml cycloheximide to stall elongation. **A** This resulted in a loss in the autocorrelation seen in Fig. 3F. **B** Monte Carlo simulations of these experiments confirm this result (although fluorescence of translation spots remains, fluctuations diminish, causing the autocorrelation to drop to zero). Sample simulated intensity fluctuations are shown in the inset. **C**,**D** Sample simulated data without added noise. Examples of these simulations can be seen in Movies S6 and S7. The insets in B correspond to the upper-most curves in C and D after simulated experimental noise is added.

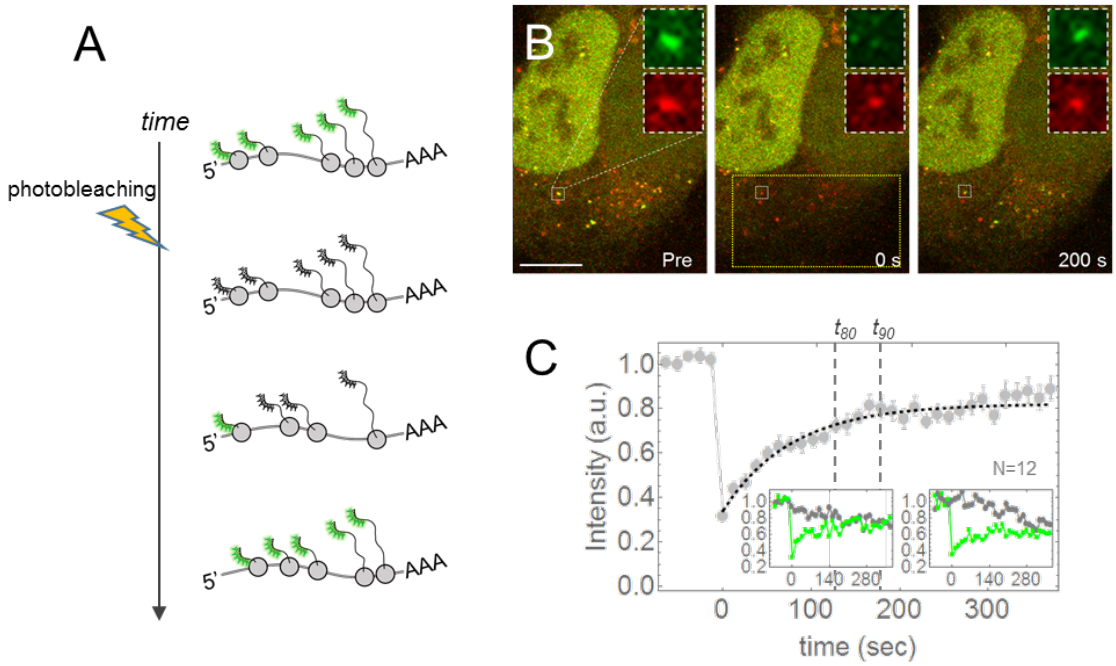

Fig. S8

A Cartoon depicting a FRAP experiment on SM-KDM5B. Initially Fab (green "Y" shapes) fully label the nascent chains emerging from the ribosomes (gray circles) that make up the polysome (mRNA shown as thicker line). Upon photobleaching, polysome fluorescence only recovers to its original value when photobleached ribosomes are replaced by newly initiated ribosomes. **B** A sample FRAP experiment in cells transiently transfected with SM-KDM5B and bead-loaded with MCP (red) and Fab (green) 6 hours earlier. The FRAP laser power was adjusted to only bleach the Fab. The image on the left shows the cell before FRAP. The middle image shows the cell immediately after photobleaching the area enclosed by the yellow box. The right frame shows the cell 200 seconds after FRAP. Insets are zoomed images of the polysome within the indicated white box. Although the Fab fluorescence photobleached, it recovered within 200 seconds. **C** Quantification of FRAP experiments like the one shown in B. The fitted 80% and 90% recovery times are shown (t_{80} and t_{90} dashed lines). The polysome fluorescence recovery was normalized to the intensity of an unbleached polysome in the same cell (dark gray curves in the examples in the inset). Depending on the polysome, recoveries could be somewhat variable, as demonstrated by the faster (left) and slower (right) recoveries in the inset. Error bars represent SEM. Scale bar, 10 µm.

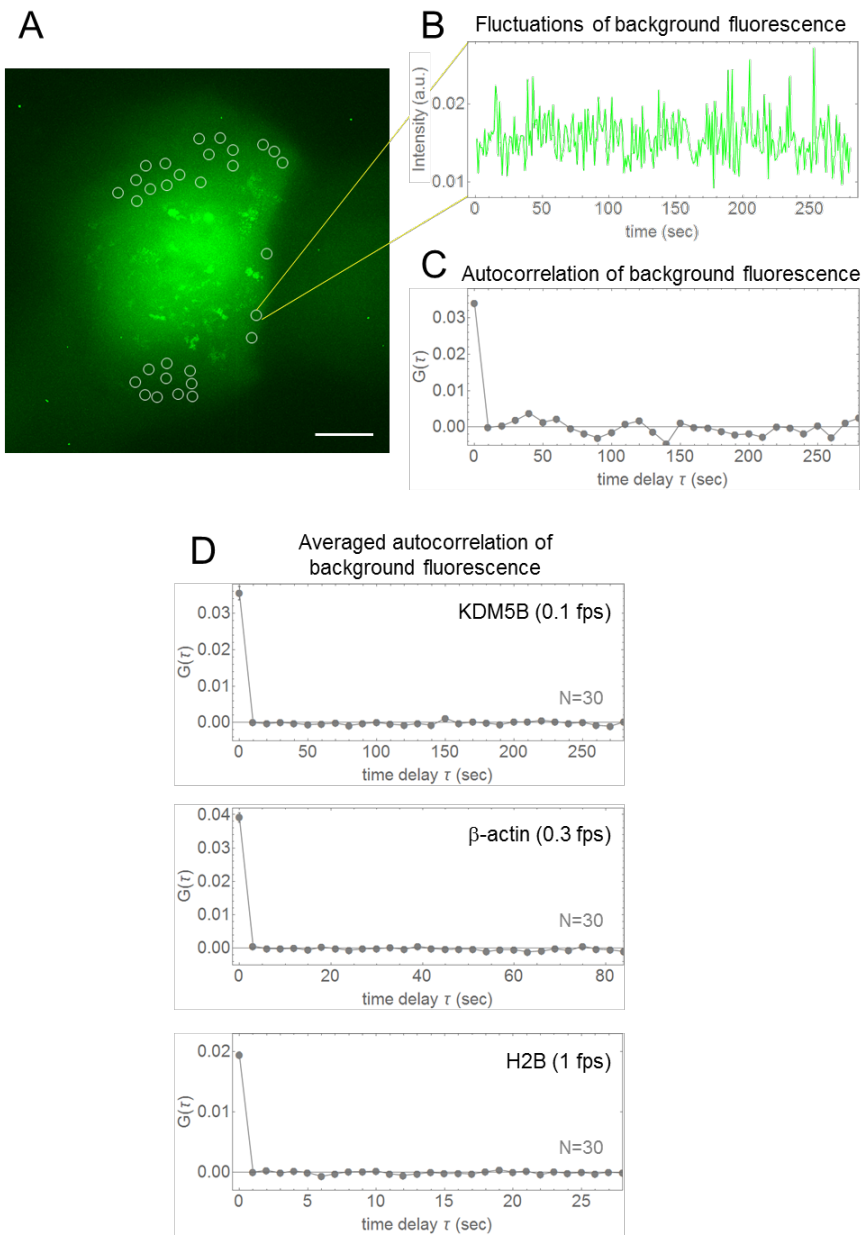

Fig. S9

To ensure background fluorescence from freely diffusing Fab and/or mature protein does not contribute to the autocorrelation of intensity fluctuations, random positions not containing any polysomes were sampled from movies of SM-KDM5B, SM-beta-actin, and SM-H2B. **A** A sample maximum intensity projection of a movie showing a cell expressing SM-KDM5B along with 30 sampled positions where polysomes were not detected. **B** The fluorescence fluctuations from one random spot. **C** The autocorrelation of the fluorescence fluctuations in B reveal little correlation. **D** The average of many such spots confirms this for the KDM5B construct (top). The same holds true for the beta-actin (middle) and H2B constructs (bottom).

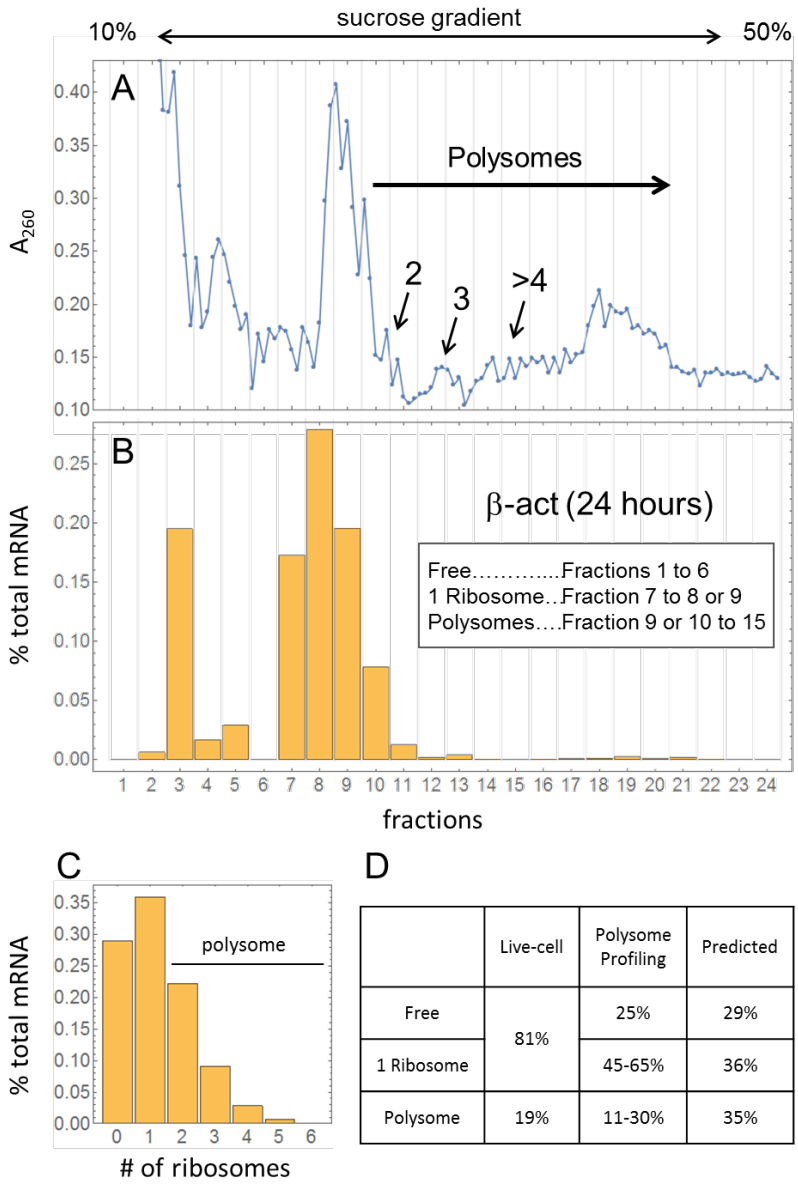

	Live-cell	Polysome Profiling	Predicted
Free	81%	25%	29%
1 Ribosome		45-65%	36%
Polysome	19%	11-30%	35%

Fig. S10

A 10-50% sucrose gradient polysome profile of cells expressing SM-beta-actin mRNA. A_{260} is the absorbance at 260 nm. The peak shows the position of the 80S single ribosome, beyond which polysome peaks are found. The rough positions of 2, 3, and >4 ribosome containing polysomes is shown. **B** qPCR against the SM-beta-actin mRNA of the individual fractions from A. **C** Predicted distribution showing the fraction of SM-beta-actin mRNA in 0, 1, 2, …, 5, 6 ribosome containing polysomes. The distribution is calculated from Sup. Eq. S2, with the ratio of elongation to initiation rates measured in live cells n = 303 ± 53 (amino acids), the length of the beta-actin transcript N = 374 (amino acids) and the number of ribosomes M = 0, 1, 2, …, 5, 6. **D** A summary table comparing the polysome profile measurements in A and B to live-cell measurements in Fig. 2E and the predictions in C.

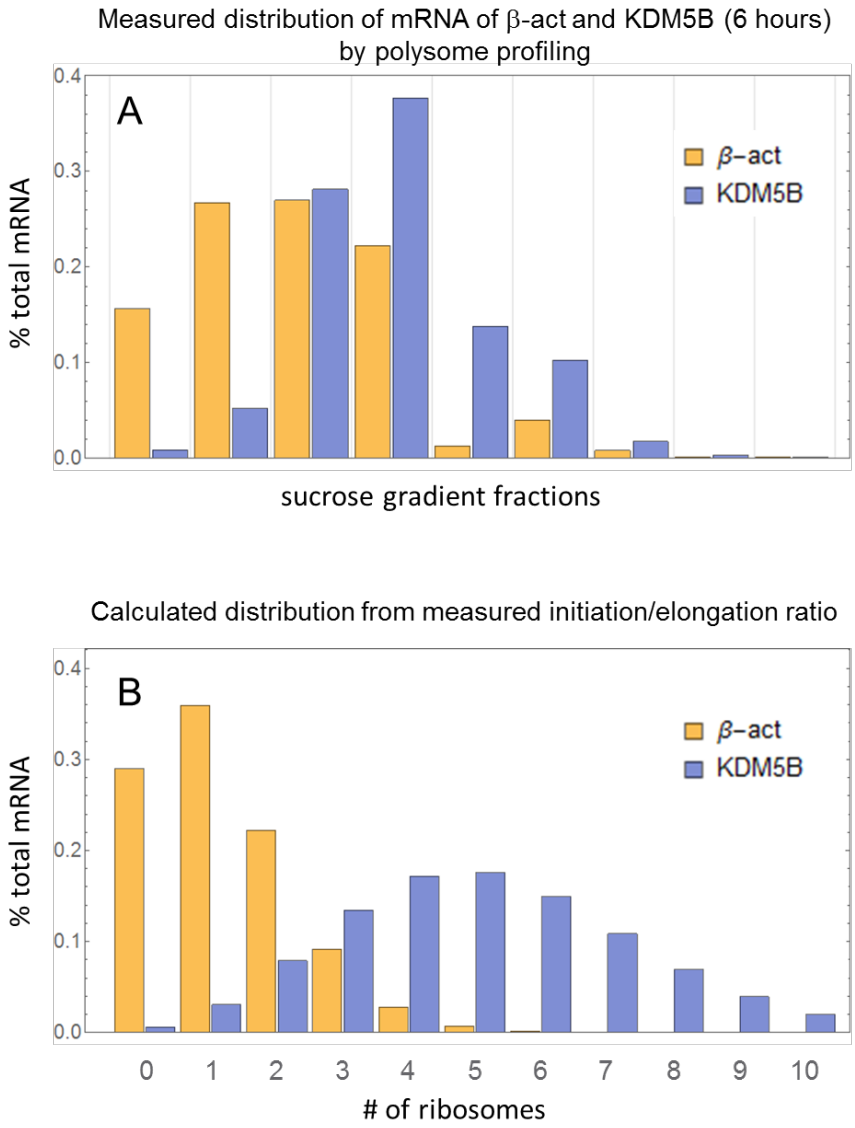

Fig. S11

A A comparison of the qPCR measured distribution of SM-beta-actin and SM-KDM5B mRNA from polysome profiling fractions. The SM-KDM5B distribution is shifted to higher fractions compared to SM-beta-actin, suggesting it is in larger polysomes. **B** Predicted distributions showing the fraction of SM-beta-actin and SM-KDM5B mRNA in 0, 1, 2, …, 5, 6 ribosome containing polysomes. The distribution is calculated from Sup. Eq. S2, with the ratio of elongation to initiation rates measured in live cells n = 303 ± 53 (amino acids), the length of the beta-actin transcript N = 374 (amino acids), the length of the KDM5B transcript N = 1544, and the number of ribosomes M = 0, 1, 2, …, 9, 10.

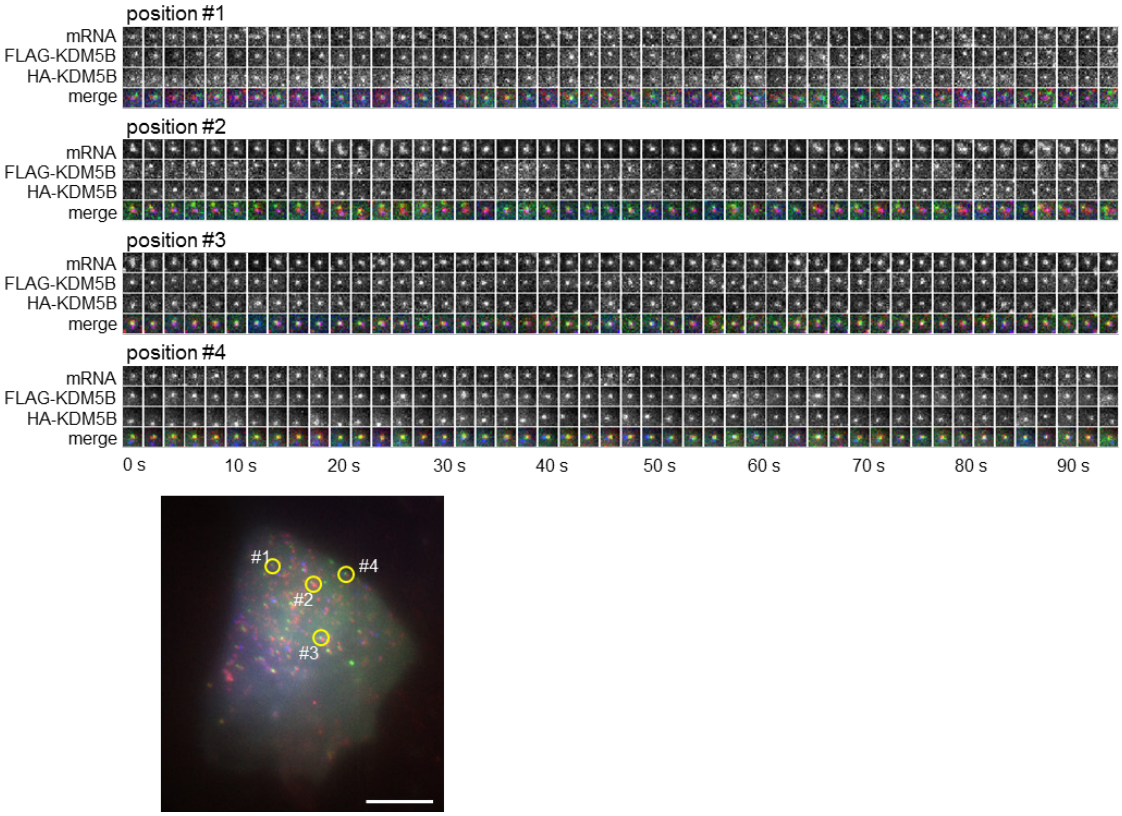

Fig. S12

Montages of four positions (#1-#4) within a single cell (shown below) where mRNA, FLAG-KDM5B, and HA-KDM5B all colocalized and co-moved, indicating multi-polysome complexes (mRNA, red; FLAG-KDM5B, green; HA-KDM5B, blue). Scale bar, 10 μm.

Movie S1

Max projection of a 13 z-stack movie showing sample SM-KDM5B polysomes imaged at one frame per second for 120 (of 300) seconds total (Ch1 red, mRNA; Ch2 green, protein).

Movie S2

Max projection of a 13 z-stack movie showing sample SM-KDM5B polysomes imaged at one frame per 1 minute for 2 hours total (Ch1 red, mRNA; Ch2 green, protein).

Movie S3

Max projection of a 13 z-stack movie of a puromycin experiment showing a loss of protein signal at SM-KDM5B polysomes compared to control cells. Cell imaged at one frame per 6.5 seconds for a total of 650 seconds (Ch1 red, mRNA; Ch2 green, protein).

Movie S4

Max projection of a 13 z-stack movie showing sample SM-beta-actin polysomes imaged at one frame per second for 120 (of 300) seconds total (Ch1 red, mRNA; Ch2 green, protein).

Movie S5

Max projection of a 13 z-stack movie showing sample SM-H2B polysomes imaged at one frame per second for 120 (of 300) seconds total (Ch1 red, mRNA; Ch2 green, protein).

Movie S6

Animated GIF of a sample stochastic Monte Carlo simulation movie of translation of SM-KDM5B transcripts. The green box shows spaghetti monster tag coding region, and the black box shows KDM5B coding region. The green circle above shows the total fluorescence intensity that would be measured at the translation site. The fluorescence time series is shown below. The x-axis is in minutes and the y-axis is in arbitrary fluorescence intensity units.

Movie S7

Animated GIF of a sample stochastic Monte Carlo simulation movie of 100 μg/ml cycloheximide stalled translation of SM-KDM5B transcripts. The green box shows spaghetti monster tag coding region, and the black box shows KDM5B coding region. The green circle above shows the total fluorescence intensity that would be measured at the translation site. The fluorescence time series is shown below. The x-axis is in minutes and the y-axis is in arbitrary fluorescence intensity units.

Movie S8

Max projection of a 13 z-stack movie showing a sample cell with two types of polysomes, FLAG-KDM5B and HA-KDM5B, labeled by Fab against the FLAG and HA tags, respectively. Cell imaged at one frame every 2 seconds for 200 seconds total (Ch1 red, mRNA; Ch2 green, FLAG; Ch3 blue, HA).

References and Notes

1. G. L. Hager, J. G. McNally, T. Misteli, Transcription dynamics. *Mol. Cell* **35**, 741–753 (2009). Medline doi:10.1016/j.molcel.2009.09.005

2. X. Darzacq, J. Yao, D. R. Larson, S. Z. Causse, L. Bosanac, V. de Turris, V. M. Ruda, T. Lionnet, D. Zenklusen, B. Guglielmi, R. Tjian, R. H. Singer, Imaging transcription in living cells. *Annu. Rev. Biophys.* **38**, 173–196 (2009). Medline doi:10.1146/annurev.biophys.050708.133728

3. J. A. Chao, Y. J. Yoon, R. H. Singer, Imaging translation in single cells using fluorescent microscopy. *Cold Spring Harb. Perspect. Biol.* **4**, a012310–a012310 (2012). Medline doi:10.1101/cshperspect.a012310

4. J. M. Halstead, T. Lionnet, J. H. Wilbertz, F. Wippich, A. Ephrussi, R. H. Singer, J. A. Chao, An RNA biosensor for imaging the first round of translation from single cells to living animals. *Science* **347**, 1367–1671 (2015). Medline doi:10.1126/science.aaa3380

5. S. Viswanathan, M. E. Williams, E. B. Bloss, T. J. Stasevich, C. M. Speer, A. Nern, B. D. Pfeiffer, B. M. Hooks, W. P. Li, B. P. English, T. Tian, G. L. Henry, J. J. Macklin, R. Patel, C. R. Gerfen, X. Zhuang, Y. Wang, G. M. Rubin, L. L. Looger, High-performance probes for light and electron microscopy. *Nat. Methods* **12**, 568–576 (2015). Medline

6. E. Bertrand, P. Chartrand, M. Schaefer, S. M. Shenoy, R. H. Singer, R. M. Long, Localization of ASH1 mRNA particles in living yeast. *Mol. Cell* **2**, 437–445 (1998). Medline doi:10.1016/S1097-2765(00)80143-4

7. J. B. Grimm, B. P. English, J. Chen, J. P. Slaughter, Z. Zhang, A. Revyakin, R. Patel, J. J. Macklin, D. Normanno, R. H. Singer, T. Lionnet, L. D. Lavis, A general method to improve fluorophores for live-cell and single-molecule microscopy. *Nat. Methods* **12**, 244–250, 3, 250 (2015). Medline doi:10.1038/nmeth.3256

8. G. Blobel, D. Sabatini, Dissociation of mammalian polyribosomes into subunits by puromycin. *Proc. Natl. Acad. Sci. U.S.A.* **68**, 390–394 (1971). Medline doi:10.1073/pnas.68.2.390

9. J. R. Warner, A. Rich, C. E. Hall, Electron microscope studies of ribosomal clusters synthesizing hemoglobin. *Science* **138**, 1399–1403 (1962). Medline doi:10.1126/science.138.3548.1399

10. A. K. Christensen, C. M. Bourne, Shape of large bound polysomes in cultured fibroblasts and thyroid epithelial cells. *Anat. Rec.* **255**, 116–129 (1999). Medline doi:10.1002/(SICI)1097-0185(19990601)255:2<116::AID-AR2>3.0.CO;2-O

11. G. Viero, L. Lunelli, A. Passerini, P. Bianchini, R. J. Gilbert, P. Bernabò, T. Tebaldi, A. Diaspro, C. Pederzolli, A. Quattrone, Three distinct ribosome assemblies modulated by translation are the building blocks of polysomes. *J. Cell Biol.* **208**, 581–596 (2015). Medline doi:10.1083/jcb.201406040

12. D. R. Larson, D. Zenklusen, B. Wu, J. A. Chao, R. H. Singer, Real-time observation of transcription initiation and elongation on an endogenous yeast gene. *Science* **332**, 475–478 (2011). Medline doi:10.1126/science.1202142

13. H. Kimura, P. R. Cook, Kinetics of core histones in living human cells: Little exchange of H3 and H4 and some rapid exchange of H2b. *J. Cell Biol.* **153**, 1341–1354 (2001). Medline doi:10.1083/jcb.153.7.1341

14. F. Mueller, T. Morisaki, D. Mazza, J. G. McNally, Minimizing the impact of photoswitching of fluorescent proteins on FRAP analysis. *Biophys. J.* **102**, 1656–1665 (2012). Medline doi:10.1016/j.bpj.2012.02.029

15. D. R. Larson, R. H. Singer, D. Zenklusen, A single molecule view of gene expression. *Trends Cell Biol.* **19**, 630–637 (2009). Medline doi:10.1016/j.tcb.2009.08.008

16. J. Yu, J. Xiao, X. Ren, K. Lao, X. S. Xie, Probing gene expression in live cells, one protein molecule at a time. *Science* **311**, 1600–1603 (2006). Medline doi:10.1126/science.1119623

17. N. T. Ingolia, S. Ghaemmaghami, J. R. S. Newman, J. S. Weissman, Genome-wide analysis in vivo of translation with nucleotide resolution using ribosome profiling. *Science* **324**, 218–223 (2009). Medline doi:10.1126/science.1168978

18. N. T. Ingolia, L. F. Lareau, J. S. Weissman, Ribosome profiling of mouse embryonic stem cells reveals the complexity and dynamics of mammalian proteomes. *Cell* **147**, 789–802 (2011). Medline doi:10.1016/j.cell.2011.10.002

19. J.-R. Yang, X. Chen, J. Zhang, Codon-by-codon modulation of translational speed and accuracy via mRNA folding. *PLOS Biol.* **12**, e1001910 (2014). Medline doi:10.1371/journal.pbio.1001910

20. R. D. Palmiter, Quantitation of parameters that determine the rate of ovalbumin synthesis. *Cell* **4**, 189–197 (1975). Medline doi:10.1016/0092-8674(75)90167-1

21. R. Jackson, N. Standart, The awesome power of ribosome profiling. *RNA* **21**, 652–654 (2015). Medline doi:10.1261/rna.049908.115

22. G. S. Wilkie, K. S. Dickson, N. K. Gray, Regulation of mRNA translation by 5′- and 3′-UTR-binding factors. *Trends Biochem. Sci.* **28**, 182–188 (2003). Medline doi:10.1016/S0968-0004(03)00051-3

23. N. Sonenberg, A. G. Hinnebusch, Regulation of translation initiation in eukaryotes: Mechanisms and biological targets. *Cell* **136**, 731–745 (2009). Medline doi:10.1016/j.cell.2009.01.042

24. Y.-W. Shieh, P. Minguez, P. Bork, J. J. Auburger, D. L. Guilbride, G. Kramer, B. Bukau, Operon structure and cotranslational subunit association direct protein assembly in bacteria. *Science* **350**, 678–680 (2015). Medline doi:10.1126/science.aac8171

25. B. Wu, C. Eliscovich, Y. Yoon, R. H. Singer, Translation dynamics of single mRNAs in live cells and neurons. *Science* 10.1126/science.aaf1084 (2016).

26. M. E. Tanenbaum, L. A. Gilbert, L. S. Qi, J. S. Weissman, R. D. Vale, A protein-tagging system for signal amplification in gene expression and fluorescence imaging. *Cell* **159**, 635–646 (2014). Medline doi:10.1016/j.cell.2014.09.039

27. T. J. Stasevich, Y. Hayashi-Takanaka, Y. Sato, K. Maehara, Y. Ohkawa, K. Sakata-Sogawa, M. Tokunaga, T. Nagase, N. Nozaki, J. G. McNally, H. Kimura, Regulation of RNA

polymerase II activation by histone acetylation in single living cells. *Nature* **516**, 272–275 (2014). Medline doi:10.1038/nature13714

28. P. L. McNeil, E. Warder, Glass beads load macromolecules into living cells. *J. Cell Sci.* **88**, 669–678 (1987). Medline

29. M. Tokunaga, N. Imamoto, K. Sakata-Sogawa, Highly inclined thin illumination enables clear single-molecule imaging in cells. *Nat. Methods* **5**, 159–161 (2008). Medline doi:10.1038/nmeth1171

30. B. P. English, R. H. Singer, A three-camera imaging microscope for high-speed single-molecule tracking and super-resolution imaging in living cells. *Proc. SPIE* **9550**, 955008 (2015).

31. A. D. Edelstein, M. A. Tsuchida, N. Amodaj, H. Pinkard, R. D. Vale, N. Stuurman, Advanced methods of microscope control using μManager software. *J. Biol. Methods* **1**, 10 (2014). Medline doi:10.14440/jbm.2014.36

32. J. Schindelin, I. Arganda-Carreras, E. Frise, V. Kaynig, M. Longair, T. Pietzsch, S. Preibisch, C. Rueden, S. Saalfeld, B. Schmid, J. Y. Tinevez, D. J. White, V. Hartenstein, K. Eliceiri, P. Tomancak, A. Cardona, Fiji: An open-source platform for biological-image analysis. *Nat. Methods* **9**, 676–682 (2012). Medline doi:10.1038/nmeth.2019

33. P. Thévenaz, U. E. Ruttimann, M. Unser, A pyramid approach to subpixel registration based on intensity. *IEEE Trans. Image Process.* **7**, 27–41 (1998). Medline doi:10.1109/83.650848